# Realizability-preserving time-stepping for the differential Reynolds stress turbulence models

T. Norddine, Martin Ferrand, S. Benhamadouche

# Highlights

**Realizability-preserving time-stepping for the differential Reynolds stress turbulence models**

T. Norddine, M. Ferrand, S. Benhamadouche

- Finite volume three-dimensional Reynolds averaged Navier–Stokes modelling of turbulent flows;
- Time stepping decomposition of differential Reynolds stress models to enforce realizability;
- Numerical verification in case of homogeneous shear flows with various initial conditions.

# Realizability-preserving time-stepping for the differential Reynolds stress turbulence models

T. Norddine[a,b,*], M. Ferrand[a,b], S. Benhamadouche[a,b]

[a] *CEREA, Ecole des Ponts, EDF R&D, 6 quai Watier, Chatou, 78400, France*
[b] *EDF R&D, Fluid Mechanics, Energy and Environment Dept., 6 quai Watier, Chatou, 78400, France*

**Abstract**

In the context of incompressible turbulence modelling, differential Reynolds stress models allow a better representation of turbulence anisotropy than classical linear eddy viscosity models and are less expensive than large eddy simulations in terms of computational cost. They rely on a modelled transport equation for the Reynolds stress tensor, which is by definition a covariance tensor and must remain symmetric positive semi-definite. However, the solution of the modelled and discretized transport equation may not preserve these mathematical properties. In the present article, a methodology to time-split Reynolds stress $\underline{\underline{R}}$ terms in the transport equation is proposed using a decomposition theorem which proves the realizability of $\underline{\underline{R}}$ provided realizable initial conditions. Realizability-preserving time-steppings are designed for several differential Reynolds stress models. The numerical schemes are presented in a finite volume context but may be used with others space discretization schemes. The realizability, precision and robustness of the numerical scheme is verified through the anisotropy time evolution in homogeneous shear-flow simulations with various initial conditions.

*Keywords:* Numerical schemes, second-order RANS, Turbulence, Realizability

## 1. Introduction

Turbulence being of a chaotic nature and involving a wide continuous range of length and time scales, it cannot be directly simulated in practice for most of practical applications. Computational resources in terms of CPU and memory would

*Corresponding author
*Email address:* thomas.norddine@edf.fr (T. Norddine)

go far beyond capabilities of the most powerful super-computers. While direct numerical simulation (DNS) considers turbulence as a deterministic phenomenon, the Reynolds averaged Navier–Stokes approach (RANS, see e.g. Pope (2000); Hanjalić and Launder (2011)) relies on a statistical description, which is cheaper in terms of computational efforts. Differential Reynolds stress models (DRSMs) offer a better prediction of the anisotropy of turbulence than linear eddy viscosity models such as the $k-\epsilon$ and $k-\omega$, especially when it comes to applications in which the walls and the shear are crucial or when dealing with additional effects in the momentum equations such as buoyancy, rotation or electromagnetic effects. The DRSMs rely on the resolution of a modelled transport equations for the Reynolds stress tensor, which is by definition the covariance matrix of the velocity fluctuation field with respect to Reynolds averaging. This tensor verifies strong mathematical properties. Schumann (1977) argued that the solutions of the DRSMs should remain symmetric semi-positive definite (SPD) tensor fields. Non SPD Reynolds stress tensors can bring the calculation to crash (see Lumley (1979, 1983)). This is similar to $\rho$ being negative for a compressible solver, or $k$ and $\varepsilon$ being negative with $k-\varepsilon$ turbulence model. Although exact transport equations do satisfy the realizability criteria by construction, most of the DRSMs, such as the LRR-IP model (Launder et al., 1975) or SSG model (Speziale et al., 1991) do not enforce their solutions to satisfy these properties at continuous level. In that respect, a few realizability preserving second-order closure turbulence models were proposed in the literature (see e.g. Shih and Lumley (1985); Shih and Shabbir (1994)). Moreover, when it comes to time and space discretization, the discrete operators may break the realizability of the discrete solutions, whatever the properties of the models. The concept of realizability stands for the preservation of all the properties of the turbulent statistical moments (here the semi-positiveness of $\underline{\underline{R}}$) while transported through modelled or discretized versions of the exact transport equations. Explicit procedures such as clipping were originally proposed to enforce realizability at the discrete level (see e.g. Deardorff (1973); Chassaing et al. (2003)). Time-stepping schemes were proposed for $k-\omega$ model by Mor-Yossef and Levy (2006), Mor-Yossef and Levy (2009), as well as for Reynolds stresses by Mor-Yossef (2014) but in a segregated manner, i.e. in which the components are solved one after the other.

In the present work, a general method is proposed to design realizability-preserving numerical schemes. The main objective of this work is to preserve, at the discrete level, the symmetry definite positiveness of the Reynolds stress tensor when the continuous solution of the model is realizable. In the case where the model and the continuous solution present some time and space domains where $\underline{\underline{R}}$ is not SPD, the realizability of the discrete solution is enforced by the numerical scheme. The proposed

schemes are implemented in the open-source CFD solver code_saturne(EDF, 2023) for DRSMs since version 6.0 and is used as the default option for DRSMs meaning that almost all the validation process dealing with second-moment is performed with this scheme including more academic and industrial test-cases: for nuclear thermal-hydraulic applications (see e.g. Dehoux et al., 2017; Mangeon et al., 2020), for atmospheric modelling (see e.g. Bahlali et al., 2020), for Lagrangian particles dispersion modelling (see e.g. Balvet et al., 2023) and for aeraulics modelling (see e.g. Amino et al., 2022). It relies on numerical time-steppings for the terms appearing in the differential Reynolds stress models, split in consistent implicit and explicit parts as long as this tensor remains realizable. The decomposition is proposed for production, dissipation and some pressure-strain correlations. The diffusion and advection by the mean flow discrete operators are shown to preserve realizability for basic finite volume schemes. The time-stepping for the terms proposed can be combined to any time and space discretization scheme for the material convection and for the diffusion terms that preserve positivity. Although realizability is an important requirement, it does not provide any guaranty when it comes to the accuracy of the numerical schemes. Indeed, by constraining non-realizable models to be realizable once discretized, robustness is improved but accuracy of the simulations might be impaired since the qualitative behavior of the model is modified. This is the reason why, accordance of the numerical simulations with analytical solutions should be investigated as well.

In that respect, the governing equations of fluid dynamics and second-order moment closure turbulence models are first presented in Section 2. The concept of realizability applied to the DRSMs is recalled in Section 3. Then, a methodology to enforce realizability at discrete level is proposed in Section 4. Realizability of the discrete solutions of a tensor advection-diffusion equation is studied in a finite volume framework. The methodology used to time-split source terms is illustrated on the standard $k-\varepsilon$ model on the decaying isotropic turbulence. A decomposition theorem for realizability preserving time-splitting of the other terms of the DRSMs is proposed and demonstrated. Decompositions in implicit and explicit parts are provided for both LRR-IP (Launder et al. (1975)) and SSG (Speziale et al. (1991)) second-moment closures.

Finally, the time-steppings implemented in code_saturne are investigated numerically. On the one hand, numerical results over verification test cases are presented in Section 5. Simulation of homogeneous shear flows, for which analytical solutions exist, are performed for investigating the realizability, the robustness and the accuracy of the proposed numerical schemes. On the other hand, the practical benefits of the realizability preserving scheme are highlighted on a validation case in Section

6, namely a turbulent flow in a cylindrical pipe with a U-bend.

## 2. Fluid dynamics and turbulence modelling

In this section, governing equations of fluid dynamics are presented in an incompressible and turbulent context. The exact mean flow and turbulent transport equations are recalled. Then, the second-moment closures LRR-IP Launder et al. (1975) and SSG Speziale et al. (1991) are provided.

### *2.1. Reynolds averaged Navier–Stokes equations*

In the Reynolds averaged Navier–Stokes (RANS) formalism, turbulent physical quantities $X$ are considered as time and space dependant random fields. They are decomposed as a Reynold's averaged term $\overline{X}$ and fluctuating part $X'$: $X = \overline{X} + X'$. In this context, the Reynolds averaged Navier–Stokes equations write:

$$\frac{\partial \rho}{\partial t} + \text{div}\ (\rho \underline{\overline{u}}) = 0, \tag{1a}$$

$$\frac{\partial \left(\rho \underline{\overline{u}}\right)}{\partial t} + \underline{\text{div}}\ (\underline{\overline{u}} \otimes \rho \underline{\overline{u}}) = -\underline{\nabla} \overline{p} + \underline{\text{div}}\ \left(\mu\ \left(\underline{\underline{\nabla}}\ \underline{\overline{u}} + \underline{\underline{\nabla}}\ \underline{\overline{u}}^T\right)\right) + \underline{\overline{f}} - \underline{\text{div}}\ \left(\rho \underline{\overline{u'} \otimes u'}\right). \tag{1b}$$

If the gravity and buoyancy are accounted for using Boussinesq approximation, the incompressible system of equations is obtained with an additional force $\underline{\overline{f}} = \rho \left(1 - \beta_0(\overline{T} - T_0)\right) \underline{g}$ in the RHS of the momentum equation (1). With $\beta_0 = \frac{1}{T_0}$ for perfect gases, $T_0$ the reference fluid temperature and $T$ the temperature of the fluid obtained from an additional internal energy equation.

In order to solve RANS equations (1), a closure law for the Reynolds stress tensor $\underline{\underline{R}} = \underline{\overline{u' \otimes u'}}$ is required. In a RANS $2^{nd}$ moment closure context, an exact transport

equation for the Reynolds stress tensor is derived:

$$\begin{aligned}\frac{\partial}{\partial t}\left(\rho\underline{\underline{R}}\right)+\underbrace{\underline{\underline{\mathrm{div}}}\left(\underline{\underline{R}}\otimes\rho\overline{\underline{u}}\right)}_{\text{Material convection}} = & \underbrace{\underline{\underline{\mathrm{div}}}\left(\mu\underline{\underline{\nabla}}\,\underline{\underline{R}}\right)}_{\text{Molecular diffusion: }\underline{\underline{D}}_{\nu}} \underbrace{-\underline{\underline{\mathrm{div}}}\left(\rho\overline{\underline{u}'\otimes\underline{u}'\otimes\underline{u}'}\right)}_{\text{Turbulent diffusion: }\underline{\underline{D}}_{t}} \\ & \underbrace{-\underline{\underline{\mathrm{div}}}\left(\overline{p'\left(\underline{u}'\otimes\underline{\underline{1}}+\underline{\underline{1}}\otimes\underline{u}'\right)}\right)}_{\text{Pressure diffusion: }\underline{\underline{D}}_{p}}+\underbrace{\overline{p'\left(\underline{\underline{\nabla}}\,\underline{u}'+\underline{\underline{\nabla}}\,\underline{u}'^{T}\right)}}_{\text{Pressure Strain Correlation: }\rho\underline{\underline{\phi}}} \\ & \underbrace{-\rho\left(\underline{\underline{\nabla}}\,\overline{\underline{u}}\cdot\underline{\underline{R}}+\underline{\underline{R}}\cdot\underline{\underline{\nabla}}\,\overline{\underline{u}}^{T}\right)}_{\text{Strain production: }\rho\underline{\underline{P}}}\underbrace{-2\overline{\mu\underline{\underline{\nabla}}\,\underline{u}'\cdot\underline{\underline{\nabla}}\,\underline{u}'^{T}}}_{\text{Dissipation rate: }\rho\underline{\underline{\varepsilon}}} \\ & \underbrace{-\rho\beta_0\left(\overline{T'\,\underline{u}'}\otimes\underline{g}+\underline{g}\otimes\overline{T'\,\underline{u}'}\right)}_{\text{Buoyancy production: }\rho\underline{\underline{G}}}.\end{aligned} \tag{2}$$

Taking half of the trace of (2) gives the exact budget of the turbulent kinetic energy $k \coloneqq \frac{1}{2}\mathrm{tr}\underline{\underline{R}}$, with production and dissipation terms defined by $P \coloneqq \frac{1}{2}\mathrm{tr}\underline{\underline{P}}$, $G \coloneqq \frac{1}{2}\mathrm{tr}\underline{\underline{G}}$ and $\varepsilon \coloneqq \frac{1}{2}\mathrm{tr}\underline{\underline{\varepsilon}}$, respectively. The integral time-scale is defined by $\tau \coloneqq \frac{k}{\varepsilon}$ and production dissipation ratio and Richardson flux number are given by $P^{\star} \coloneqq \frac{P}{\varepsilon}$ and $G^{\star} \coloneqq \frac{G}{\varepsilon}$.

### *2.2. Second moment turbulent closure modelling*

Several terms such as the pressure strain correlations, triple correlations or turbulent dissipation tensor arising in the Reynolds stress transport equation (2) cannot be computed from resolved quantities and require modelling. Furthermore, if buoyancy effects are accounted for, an additional $\underline{\underline{G}}$ term[1] arises in equation (2) but will be omitted in the following. Closures yield DRSM of the general form:

$$\frac{\partial}{\partial t}\left(\rho\underline{\underline{R}}\right)+\underline{\underline{\mathrm{div}}}\left(\underline{\underline{R}}\otimes\rho\overline{\underline{u}}\right)=\rho\left(\underline{\underline{P}}+\underline{\underline{\Phi}}-\underline{\underline{\varepsilon}}\right)+\underline{\underline{D}}. \tag{3}$$

[1]If buoyancy effects are accounted for, the velocity–temperature correlations can be modelled through generalized gradient diffusion hypothesis (GGDH):

$$\underline{\underline{G}}\simeq-\beta_0 C_S\frac{k}{\varepsilon}\left(\underline{g}\otimes\underline{\underline{R}}\cdot\underline{\nabla}\overline{T}+\underline{\underline{R}}\cdot\underline{\nabla}\overline{T}\otimes\underline{g}\right).$$

with $C_S = 0.236$.

The aim of the present article is not to give a complete review of all existing models (see e.g. Pope (2000) for a valuable presentation) but to design some time discretization rules for the modelled terms. The following closures are considered in the present work:

*Diffusion terms.* $\underline{\underline{D}} = \underline{\underline{D}}_t + \underline{\underline{D}}_p + \underline{\underline{D}}_\nu$ can be modelled with both isotropic or anisotropic diffusion closures. The simple gradient diffusion hypothesis (SGDH, Shir (1973)) is considered in the present work as an illustration but can be extended to anisotropy models:

$$\underline{\underline{D}}_p + \underline{\underline{D}}_t \simeq \underline{\underline{\mathrm{div}}} \left( C_S \, \rho \frac{k^2}{\varepsilon} \underline{\underline{\nabla}} \, \underline{\underline{R}} \right). \tag{4}$$

*The dissipation tensor.* $\underline{\underline{\varepsilon}}$ can be assumed to be locally isotropic (see Pope (2000)):

$$\underline{\underline{\varepsilon}} \simeq \frac{2}{3} \varepsilon \, \underline{\underline{1}}. \tag{5}$$

The dissipation rate $\varepsilon$ is obtained from the following modelled transport equation:

$$\frac{\partial (\rho \varepsilon)}{\partial t} + \mathrm{div} \, (\varepsilon \rho \, \underline{\overline{u}}) = \mathrm{div} \left( \left( \mu \underline{\underline{1}} + \rho C_\varepsilon \frac{k}{\varepsilon} \underline{\underline{R}} \right) \cdot \underline{\nabla} \varepsilon \right) + \rho \frac{\varepsilon}{k} \left( C_{\varepsilon 1} P - C_{\varepsilon 2} \varepsilon \right). \tag{6}$$

The model's constants are provided in Table 1.

| $C_\varepsilon$ | $C_{\varepsilon 1}$ | $C_{\varepsilon 2}$ |
|---|---|---|
| 0.18 | 1.44 | 1.92 |

Table 1: Constants for the $\varepsilon$ equation.

*Pressure correlation term.* $\underline{\underline{\Phi}}$ is modelled thanks to high-Reynolds number models LRR-IP (Launder et al., 1975) and SSG (Speziale et al., 1991). However, the proposed methodology to time-discretize model terms can be extended to other closures.

(a) **Linear return to isotropy LRR-IP model** rely on the slow term proposed by Rotta (1951) and the Isotropization of Production (IP, Naot et al. (1970)).

$$\underline{\underline{\Phi}} = \underline{\underline{\Phi}}_s + \underline{\underline{\Phi}}_r = -C_1 \frac{\varepsilon}{k} \underline{\underline{R}}^D - C_2 \underline{\underline{P}}^D, \tag{7}$$

where $\underline{\underline{A}}^D \coloneqq \underline{\underline{A}} - \frac{1}{3} (\mathrm{tr} \underline{\underline{A}}) \underline{\underline{1}}$ denotes the deviatoric part of tensor $\underline{\underline{\mathrm{A}}}$. The LRR-IP model constants are provided in Table 2.

| $C_1$ | $C_2$ | $C_S$ |
|---|---|---|
| 1.80 | 0.60 | 0.22 |

Table 2: LRR-IP model constants from Launder et al. (1975).

(b) **Non-linear SSG model** is a sum of rapid $\underline{\underline{\Phi}}_r$ and slow $\underline{\underline{\Phi}}_s$ terms defined as:

$$\underline{\underline{\Phi}} = \underline{\underline{\phi}}_{s,1} + \underline{\underline{\phi}}_{s,2} + \underline{\underline{\phi}}_{r,1} + \underline{\underline{\phi}}_{r,2} + \underline{\underline{\phi}}_{r,3} + \underline{\underline{\phi}}_{r,4}, \tag{8}$$

$$\underline{\underline{\phi}}_{s,1} = -C_{s,1}\frac{\varepsilon}{k}\underline{\underline{R}}^D, \tag{9}$$

$$\underline{\underline{\phi}}_{s,2} = C_{s,2}\frac{\varepsilon}{k^2}\left(\underline{\underline{R}}^D \cdot \underline{\underline{R}}^D - \frac{1}{3}\mathrm{tr}(\underline{\underline{R}}^D \cdot \underline{\underline{R}}^D)\underline{\underline{1}}\right), \tag{10}$$

$$\underline{\underline{\phi}}_{r,1} = -C_{r,1}\frac{P}{k}\underline{\underline{R}}^D, \tag{11}$$

$$\underline{\underline{\phi}}_{r,2} = \left(C_{r,2} - \frac{C_{r,3}}{k}\sqrt{\mathrm{tr}(\underline{\underline{R}}^D \cdot \underline{\underline{R}}^D)}\right) k\underline{\underline{S}}, \tag{12}$$

$$\underline{\underline{\phi}}_{r,3} = C_{r,4}\left(\underline{\underline{R}}^D \cdot \underline{\underline{S}} + \underline{\underline{S}} \cdot \underline{\underline{R}}^D - \frac{2}{3}\mathrm{tr}(\underline{\underline{R}}^D \cdot \underline{\underline{S}})\underline{\underline{1}}\right), \tag{13}$$

$$\underline{\underline{\phi}}_{r,4} = C_{r,5}\left(\underline{\underline{\Omega}} \cdot \underline{\underline{R}}^D - \underline{\underline{R}}^D \cdot \underline{\underline{\Omega}}\right) = C_{r,5}\left(\underline{\underline{\Omega}} \cdot \underline{\underline{R}} - \underline{\underline{R}} \cdot \underline{\underline{\Omega}}\right). \tag{14}$$

SSG model's constants are presented in Table 3.

| $C_S$ | $C_{s,1}$ | $C_{s,2}$ | $C_{r,1}$ | $C_{r,2}$ | $C_{r,3}$ | $C_{r,4}$ | $C_{r,5}$ |
|---|---|---|---|---|---|---|---|
| 0.22 | 1.70 | 1.05 | 0.90 | 0.80 | 0.65 | 0.625 | 0.20 |

Table 3: SSG model constants from Speziale et al. (1991).

## 3. Realizability of the Reynolds stress tensor

In fluid mechanics, governing equations obey to mathematical and physical requirements such as positivity for temperature and scalar concentration. Turbulent quantities such as the Reynolds stress tensor and the turbulent fluxes also verify physical and mathematical properties, inherent to their definition as statistical averages. They verify transport equations derived from mass, momentum and energy balance.

Fortunately, properties related to these quantities are preserved while transported through unclosed equations. For physical and numerical reasons, the modelled equations should preserve properties of the unclosed equations, such as the positivity of the Reynolds stress tensor. The concept of realizability stands for the preservation of all the properties of the statistical moments by the solution of the modelled URANS equations. This concept is exposed in the present section for the Reynolds stress tensor, only. Realizability will be used in a more restricted way in the following, meaning positivity of the Reynolds stress tensor. The interested reader may refer to Appendix A for further details regarding the realizability of the exact and modelled equations.

### *3.1. Realizability of the Reynolds stress tensor*

For the Reynolds stress tensor to be realizable, Schumann (1977) argued that the following requirements should be fulfilled:

$$R_{\alpha\alpha} \geq 0, \qquad \alpha \in \{1,2,3\}, \tag{15a}$$

$$R_{\alpha\alpha}R_{\beta\beta} - R_{\alpha\beta}^2 \geq 0, \qquad (\alpha,\beta) \in \{1,2,3\}^2, \tag{15b}$$

$$\det \underline{\underline{R}} \geq 0, \tag{15c}$$

where Einstein's convention holds for Latin indices only. Requirement (15a) corresponds to the velocity field being real and kinetic energy being non-negative. Since $\underline{\underline{R}}$ is a covariance matrix, (15b) corresponds to the Cauchy–Schwarz inequality. Finally criterion (15c) arises from definition of the Reynolds stress tensor as a Reynold's average (see Schumann (1977) for a proof). This definition is equivalent to $\underline{\underline{R}}$ being a symmetric semi-positive definite tensor.

In an invariant modelling context, the Reynolds stress tensor transport equations may be equivalently expressed in terms of turbulent kinetic energy and turbulent anisotropy tensor. Provided positive turbulent kinetic energy, realizability of the Reynolds stress tensor can be studied with respect to the turbulent anisotropy tensor $\underline{\underline{b}}$:

$$\underline{\underline{b}} \coloneqq \frac{1}{2k}\underline{\underline{R}} - \frac{1}{3}\underline{\underline{I}} = \frac{1}{2k}\underline{\underline{R}}^D. \tag{16}$$

Since $\underline{\underline{b}}$ is a zero-trace symmetric tensor, using Caylay–Hamilton theorem, Lumley (1979) showed that the only non-trivial linearly independent scalar invariants of $\underline{\underline{b}}$ are $I_2$ and $I_3$, defined as:

$$I_2 \coloneqq -\frac{1}{2}\mathrm{tr}(\underline{\underline{b}} \cdot \underline{\underline{b}}), \qquad I_3 \coloneqq \frac{1}{3}\mathrm{tr}(\underline{\underline{b}} \cdot \underline{\underline{b}} \cdot \underline{\underline{b}}). \tag{17}$$

Provided positive turbulent kinetic energy, realizability of the Reynolds stress tensor requires that invariants $(I_3,-I_2)$ belong to the closed and bounded set $\Omega_{\text{Lumley},1}$:

$$\Omega_{\text{Lumley},1} = \left\{ (I_2, I_3) \in \mathbb{R}^2, \quad 3\left(\frac{|I_3|}{2}\right)^{\frac{2}{3}} \leq -I_2 \leq \frac{1}{9}\left(1 + 27 I_3\right), \quad I_3 \in \left[-\frac{1}{108}, \frac{2}{27}\right] \right\}. \tag{18}$$

However, for a better readability, Pope (2000) proposed another graphical representation with respect to $\xi$ and $\eta$:

$$6\eta^2 = -2I_2, \quad 6\xi^3 = 3I_3. \tag{19}$$

For $\underline{\underline{R}}$ to be realizable provided a positive turbulent kinetic energy $k$, $\xi$ and $\eta$ should belong to the bounded closed set $\Omega_{\text{Lumley},2}$ (Lumley's triangle - Figure 1):

$$\Omega_{\text{Lumley},2} = \left\{ (\xi, \eta) \in \mathbb{R}^2, \quad |\xi| \leq \eta \leq \sqrt{\frac{1}{27} + 2\xi^3}, \quad \xi \in \left[-\frac{1}{6}, \frac{1}{3}\right] \right\}. \tag{20}$$

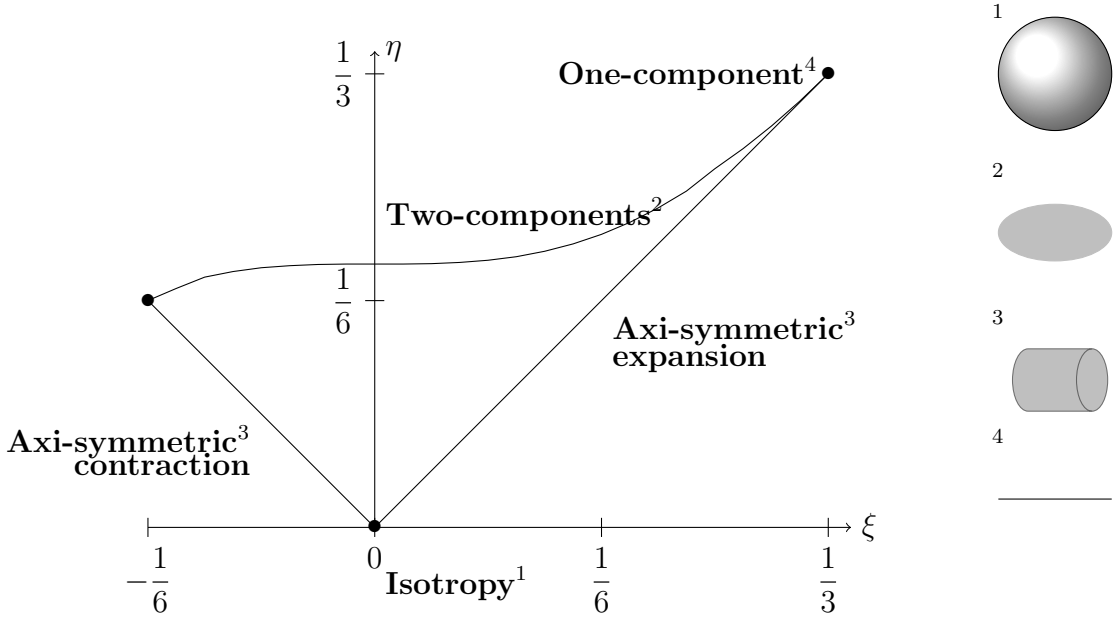


Figure 1: Lumley Triangle in $(\xi, \eta)$ plane.

## 4. Numerical methods to enforce realizability

Solutions of the DRSM such as the SSG and LRR-IP models are *a priori* non-realizable as recalled in Appendix A. That means that there exist some solutions of these models at the continuous level such that it exists a time and space domain where the solutions are not SPD. Realizability may be enforced at a discrete level through numerical methods such as clippings (see Deardorff (1973); Chassaing et al. (2003)). However, these methods are discarded in the present work since they may dramatically impair the conservation of the kinetic energy and its physical meaning. Our approach consists in designing realizability preserving numerical schemes instead. First of all, realizability of the DRSM is studied in a finite volume context by considering a tensor advection-diffusion equation. Then, a decomposition theorem for the time-splitting of the right-hand-side terms is proposed. This decomposition is shown to preserve the realizability of the discrete solutions, while departing from realizable initial conditions. We emphasise that the proposed methodology can be applied to any (realizable or not) models once one proposes a time decomposition that fulfils theorem 1.

### *4.1. Realizability of advection diffusion equations with finite volume methods*

As a first step, right-hand side (RHS) terms are discarded and the realizability of the advection diffusion equations for tensor $\underline{\underline{R}}$ is studied analytically in a finite volume framework along with the Shir model:

$$\frac{\partial\left(\rho\underline{\underline{R}}\right)}{\partial t}+\underline{\underline{\mathrm{div}}}\left(\underline{\underline{R}}\otimes\rho\underline{u}\right)-\underline{\underline{\mathrm{div}}}\left(\left(\mu+C_S\rho\frac{k^2}{\varepsilon}\right)\underline{\underline{\nabla}}\,\underline{\underline{R}}\right)=\underline{\underline{0}}. \tag{21}$$

The homogeneous diffusion coefficient obtained through simple gradient diffusion hypothesis is denoted as: $\tilde{\mu}=\left(\mu+C_S\rho\frac{k^{n\,2}}{\varepsilon^n}\right)\geq 0$. Boundary conditions are omitted and domain $\Omega\times[0,T]$ is discretized in $N_{cells}$ cells and $N_T$ time steps.

Let us consider a given cell $c$ of volume $V_c$. The set of faces $f$ of measure $S_f$ are split into boundary faces $f_{c|b}$ and internal faces $\left(f_{c|\tilde{c}}\right)_{\tilde{c}\in\mathcal{C}_c}$, associated to cell $c$. The set of inner faces associated to $c$ is denoted by $\mathcal{F}_c$ and the set of neighboring cells $\tilde{c}\in\mathcal{C}_c$ (connected by an interior face $f_{c|\tilde{c}}$ to cell $c$). For the sake of clarity, we consider either Dirichlet boundary conditions on the set of boundary faces of $c$ denoted by $\mathcal{F}_c^b$ or homogeneous Neumann boundary conditions.

Then, $\underline{x}_c$, $\underline{x}_{\tilde{c}}$ and $\underline{x}_{f_{c|\tilde{c}}}$ stands for the center of gravity of cell $c$, neighboring cells $\tilde{c}\in\mathcal{C}_c$ and faces $\left(f_{c|\tilde{c}}\right)_{\tilde{c}\in\mathcal{C}_c}$, respectively. In a finite volume context, the cell, face and

time averages of quantity $(\cdot)$ are respectively defined by:

$$(\cdot)_c \coloneqq \frac{1}{V_c}\int_c (\cdot)\ \mathrm{d}\Omega,\ (\cdot)_f \coloneqq \frac{1}{S_f}\int_f (\cdot)\ \mathrm{d}S,\ (\cdot)|_n^{n+1} \coloneqq \frac{1}{\Delta t}\int_n^{n+1} (\cdot)\ \mathrm{d}t. \tag{22}$$

Integrating equation (21) over cell $c$ and time range $[t^n, t^{n+1}[$ leads to the definition of the extensive quantities, $V_c$ the cell volume and $M_c$ cell mass(they are denoted by capital letters):

$$\begin{aligned} V_c &\coloneqq \int_c \mathrm{d}\Omega, \\ M_c &\coloneqq \int_c \rho \mathrm{d}\Omega. \end{aligned} \tag{23}$$

As for the intensive quantities, let $\rho_c$ be the cell-averaged density, and let $\underline{\underline{R}}_c$ be the density-weighted cell-averaged Reynolds stress tensor, defined as:

$$\begin{aligned} \rho_c &\coloneqq \frac{M_c}{V_c}, \\ \underline{\underline{R}}_c &\coloneqq \frac{\left(\rho \underline{\underline{R}}\right)_c}{\rho_c}, \end{aligned} \tag{24}$$

and extensive face mass flux going from cell $c$ to $\tilde{c}$:

$$\dot{M}_{c>\tilde{c}} \coloneqq (\rho \underline{u})_f \cdot \underline{S}_{c>f}. \tag{25}$$

Then, approximating the outgoing convective numerical flux of (21) through face $f$ and time interval $[t^n,\, t^{n+1}[$ gives $\left(\underline{\underline{R}} \otimes \rho \underline{u}\right)_f \Big|_n^{n+1} \cdot \underline{S}_{c>f} \approx \underline{\underline{R}}_f \Big|_n^{n+1} \dot{M}_{c>f} \Big|_n^{n+1}$, and using cell mass balance $M_c^{n+1} - M_c^n = -\sum_{f\in\mathcal{F}_c} \dot{M}_{c>f} \Big|_n^{n+1}$, yields the resulting finite volume numerical scheme presented in equation (26).

$$M_c^n \underline{\underline{R}}_c^{n+1} + \Delta t \sum_{f\in\mathcal{F}_c} \left( \left( \underline{\underline{R}}_f \Big|_n^{n+1} - \underline{\underline{R}}_c^{n+1} \right) \dot{M}_{c>f} \Big|_n^{n+1} - \tilde{\mu}_f \underline{\underline{\nabla}}\, \underline{\underline{R}}_f \Big|_n^{n+1} \cdot \underline{S}_{c>f} \right) = M_c^n \underline{\underline{R}}_c^n. \tag{26}$$

A $\theta$ time-stepping is used:

$$\underline{\underline{R}}_f \Big|_n^{n+1} = \theta \underline{\underline{R}}_f^{n+1} + (1-\theta) \underline{\underline{R}}_f^n. \tag{27}$$

In the latter, an implicit Euler scheme ($\theta = 1$) is considered for both convection and

diffusion discrete operators for the sake of simplicity for the realizabilty proof[2].

Upwind fluxes for the convective scheme are considered[3], which provides the following definition for Reynolds stress tensor at an interior face $f_{c|\tilde{c}}$ and a Dirichlet boundary face $f_{c|b}$:

$$\underline{\underline{R}}_{f_{c|\tilde{c}}}\ \dot{M}_{c>\tilde{c}}\Big|_n^{n+1} = \underline{\underline{R}}_{c}\ \dot{M}^{+}_{c>\tilde{c}}\Big|_n^{n+1} + \underline{\underline{R}}_{\tilde{c}}\ \dot{M}^{-}_{c>\tilde{c}}\Big|_n^{n+1}, \tag{28}$$

$$\underline{\underline{R}}_{f_{c|b}}\ \dot{M}_{c>f_{c|b}}\Big|_n^{n+1} = \underline{\underline{R}}_{c}\ \dot{M}^{+}_{c>\tilde{c}}\Big|_n^{n+1} + \underline{\underline{R}}^{Imp}_{f_{c|b}}\ \dot{M}^{-}_{c>f_{c|b}}\Big|_n^{n+1}, \tag{29}$$

where $\dot{M}^{+}_{c>\tilde{c}}\Big|_n^{n+1} := \max\left(\dot{M}_{c>\tilde{c}}\Big|_n^{n+1}, 0\right)$ and $\dot{M}^{-}_{c>\tilde{c}}\Big|_n^{n+1} := \min\left(\dot{M}_{c>\tilde{c}}\Big|_n^{n+1}, 0\right)$ and $\underline{\underline{R}}^{Imp}_{f_{c|b}}$ is the imposed value, mandatory for in-going mass flux faces.

Iterative two-point flux approximation is considered for the discrete diffusion operator (see Ferrand et al. (2014) for more details) which reads for inner and Dirichlet boundary faces:

$$\tilde{\mu}_{f_{c|\tilde{c}}}\underline{\underline{\nabla}}\ \underline{\underline{R}}_{f_{c|\tilde{c}}} \cdot \underline{S}_{c>\tilde{c}} \approx \frac{\tilde{\mu}_{f_{c|\tilde{c}}} S_{f_{c|\tilde{c}}}}{d_{f_{c|\tilde{c}}}} \left(\underline{\underline{R}}_{\tilde{c}} - \underline{\underline{R}}_{c}\right), \tag{30}$$

$$\tilde{\mu}_{f_{c|b}}\underline{\underline{\nabla}}\ \underline{\underline{R}}_{f_{c|b}} \cdot \underline{S}_{c>f_{c|b}} \approx \frac{\tilde{\mu}_{f_{c|b}} S_{f_{c|b}}}{d_{f_{c|b}}} \left(\underline{\underline{R}}^{Imp}_{f_{c|b}} - \underline{\underline{R}}_{c}\right), \tag{31}$$

where the face viscosities are approximated by: $\tilde{\mu}_{f_{c|\tilde{c}}} = \frac{\tilde{\mu}_c \tilde{\mu}_{\tilde{c}}}{\alpha_{c>\tilde{c}}\tilde{\mu}_c + (1-\alpha_{c>\tilde{c}})\tilde{\mu}_{\tilde{c}}}$, the $\tilde{\mu}_{f_{c|b}} = \tilde{\mu}_c$, cell-cell distance by $d_{f_{c|\tilde{c}}} = \frac{\underline{x}_{\tilde{c}} - \underline{x}_c}{S_{f_{c|\tilde{c}}}} \cdot \underline{S}_{c>\tilde{c}}$, the cell-boundary face distance by $d_{f_{c|b}} = \frac{\underline{x}_{f_{c|b}} - \underline{x}_c}{S_{f_{c|b}}} \cdot \underline{S}_{c>f_{c|b}}$ and the geometric weighted factor by $\alpha_{c>\tilde{c}}$ is defined as: $\frac{\left(\underline{x}_{f_{c|\tilde{c}}} - \underline{x}_{\tilde{c}}\right)\cdot \underline{S}_{c>\tilde{c}}}{(\underline{x}_c - \underline{x}_{\tilde{c}})\cdot \underline{S}_{c>\tilde{c}}}$.

Assembling the finite volume scheme for the advection diffusion transport equation reads in the bloc-matrix form, for all cells $c \in [1;\ N_{cells}]$:

$$\sum_{\tilde{c}\in[1;\ N_{cells}]} A^n_{c\tilde{c}} \underline{\underline{R}}^{n+1}_{\tilde{c}} = \underline{\underline{B}}^n_c, \tag{32}$$

[2]Obviously a CFL and a Fourier conditions on the time step would appear for a $\theta$-scheme with $\theta < 1$.

[3]This choice is made only for the sake of simplicity for the realizability proof, other convective schemes are available in code_saturne.

with matrix $\mathbf{A}^n$ diagonal and off-diagonal components given by:

$$\begin{aligned}
A^n_{c\tilde{c}} = \quad & M^n_c \quad + \Delta t \sum_{f_{c|\tilde{c}} \in \mathcal{F}_c} \left( \frac{\tilde{\mu}_{f_{c|\tilde{c}}} S_{f_{c|\tilde{c}}}}{d_{f_{c|\tilde{c}}}} - \dot{M}^-_{c>\tilde{c}} \Big|_n^{n+1} \right) \quad \text{, if } c = \tilde{c} \\
A^n_{c\tilde{c}} = \quad & \qquad - \Delta t \qquad \left( \frac{\tilde{\mu}_{f_{c|\tilde{c}}} S_{f_{c|\tilde{c}}}}{d_{f_{c|\tilde{c}}}} - \dot{M}^-_{c>\tilde{c}} \Big|_n^{n+1} \right) \quad \text{, if } \tilde{c} \in \mathcal{C}_c, \\
A^n_{c\tilde{c}} = \quad & \qquad 0 \qquad\qquad\qquad\qquad\qquad\qquad\qquad\qquad\quad \text{, otherwise.}
\end{aligned} \tag{33}$$

and the RHS is composed of symmetric positive definite (SPD) tensors for all cell indexes:

$$\underline{\underline{B}}^n_c = M^n_c \underline{\underline{R}}^n_c + \Delta t \left( \sum_{f_{c|b} \in \mathcal{F}^b_c} \left( \frac{\tilde{\mu}_{f_{c|b}} S_{f_{c|b}}}{d_{f_{c|b}}} - \dot{M}^-_{c>f_{c|b}} \Big|_n^{n+1} \right) \underline{\underline{R}}^{Imp}_{f_{c|b}} \right). \tag{34}$$

It is clear that off-diagonal terms of $\mathbf{A}^n$ are negative and $\mathbf{A}^n$ is diagonal dominant. Thus $\mathbf{A}^n$ is a M-matrix and is invertible and all the entries of $(\mathbf{A}^n)^{-1}$ are non-negative:

$$\begin{pmatrix} \underline{\underline{R}}^{n+1}_1 \\ \vdots \\ \underline{\underline{R}}^{n+1}_{N_{cells}} \end{pmatrix} = (\mathbf{A}^n)^{-1} \begin{pmatrix} \underline{\underline{B}}^n_1 \\ \vdots \\ \underline{\underline{B}}^n_{N_{cells}} \end{pmatrix}. \tag{35}$$

Let us assume Reynolds stress tensor field being realizable at time step $t^n$ and at Dirichlet boundaries, i.e. $M_c \underline{\underline{R}}^n_c$ is SPD for all $c$ in $\{1, \ldots, N_{cells}\}$ and so are $\underline{\underline{R}}^{Imp}_{f_{c|b}}$ for all Dirichlet boundary faces, so $\underline{\underline{B}}^n_c$ is SPD. All coefficients of the matrix $(\mathbf{A}^n)^{-1}$ are non-negative. Hence $\underline{\underline{R}}^{n+1}_c$ is a linear combination of SPD tensors with positive coefficients. As a consequence $\underline{\underline{R}}^{n+1}_c$ is SPD for all $c$ in $\{1, \ldots, N_{cells}\}$ without any CFL condition. The numerical scheme preserves the realizability of the discrete tensor field.

*4.2. Illustration of the methodology with a realizable time-stepping for $k - \varepsilon$*

The purpose of the present article is to deal with RHS terms of equation (3). As a first step, to illustrate the methodology of RHS term time-splitting, we go back in this section on the well known treatment of the $k - \varepsilon$ model (see Mohammadi and Pironneau (1993) for a complete presentation). Let us consider, for the sake of simplicity, the case of decaying homogeneous isotropic turbulence, the $k - \varepsilon$ model

gives:

$$\frac{\mathrm{d}k}{\mathrm{d}t} = -\varepsilon, \qquad \frac{\mathrm{d}\varepsilon}{\mathrm{d}t} = -C_{\varepsilon 2}\frac{\varepsilon}{\tau}, \tag{36}$$

with initial conditions $k(t=0) = k_0 > 0$, $\varepsilon(t=0) = \varepsilon_0 > 0$ so that the integral timescale $\tau \coloneqq \frac{k}{\varepsilon}$ is also positive at initial time. The analytical solutions for $k$, $\varepsilon$ and $\tau$ are obtained, respectively,

$$\frac{k}{k_0} = \left(\frac{\tau}{\tau_0}\right)^{\frac{-1}{C_{\varepsilon 2}-1}}, \qquad \frac{\varepsilon}{\varepsilon_0} = \left(\frac{\tau}{\tau_0}\right)^{\frac{-C_{\varepsilon 2}}{C_{\varepsilon 2}-1}}, \qquad \tau(t) = \tau_0 + (C_{\varepsilon 2}-1)t. \tag{37}$$

The analytical solutions of the model obviously fulfill the realizability conditions $k > 0$ and $\varepsilon > 0$ since $C_{\varepsilon 2} > 1$. It is instructive to analyse whether basic time-schemes also verify the realizability condition. Let us start with the explicit Euler scheme:

$$\frac{k^{n+1}-k^n}{\Delta t} = -\varepsilon^n, \qquad \frac{\varepsilon^{n+1}-\varepsilon^n}{\Delta t} = -C_{\varepsilon 2}\frac{\varepsilon^n}{\tau^n}, \tag{38}$$

which is realizable if and only if the following condition holds: $1 > C_{\varepsilon 2}\frac{\Delta t}{\tau^n}$. The coupled implicit Euler version (39) is realizable without any restriction, since again $C_{\varepsilon 2} > 1$.

$$\frac{k^{n+1}-k^n}{\Delta t} = -\varepsilon^{n+1}, \qquad \frac{\varepsilon^{n+1}-\varepsilon^n}{\Delta t} = -C_{\varepsilon 2}\frac{\varepsilon^{n+1}}{\tau^n}. \tag{39}$$

However, it requires a coupled resolution of $k$ and $\varepsilon$. Finally, let us consider a segregated realizability preserving time-stepping, with both destruction terms on the RHS of $k$ and $\varepsilon$ equations, which are made implicit with respect to the resolved variable[4]:

$$\frac{k^{n+1}-k^n}{\Delta t} = -\frac{k^{n+1}}{\tau^n}, \qquad \frac{\varepsilon^{n+1}-\varepsilon^n}{\Delta t} = -C_{\varepsilon 2}\frac{\varepsilon^{n+1}}{\tau^n}. \tag{40}$$

Time-stepping (40) is coherent with the analytical solution in the sense that $\tau$ varies linearly over time whereas $k$ and $\varepsilon$ decay exponentially.

An illustration of the time integration of the numerical schemes is provided in

[4]Positive production terms would be treated explicit in time.

Figure 2 (left) for the $k$ variable. The simulations ran for 200 seconds and we considered an initial state with $k_0 = 1\,\mathrm{m}^2\,\mathrm{s}^{-2}$, $\varepsilon_0 = 1\,\mathrm{m}^2\,\mathrm{s}^{-3}$ so that $\tau_0 = 1\,\mathrm{s}$. The time step is: $\Delta t = 1.1 > \dfrac{\tau_0}{C_{\varepsilon,2}} > \tau_0$. The Euler explicit scheme is shown to break the realizability since $k$ gets negative. Furthermore, the numerical error defined as:

$$err = \max_{1<n<N} \left( ||k(t_n) - k^n||_{l_2} \right), \tag{41}$$

is drawn, with $k(t_n)$ the exact solution at time $t_n = n \cdot \Delta t$, $k^n$ the numerical solution at time $t_n$, and $|| \cdot ||_{l_2}$ the discrete $l_2$ norm. The realizability-preserving scheme is shown to be accurate and unconditionally realizable for this problem. The Euler implicit scheme also preserves the realizability of the solutions of this test case but it is less accurate than the realizability-preserving one and requires a coupled resolution of $k$ and $\varepsilon$.

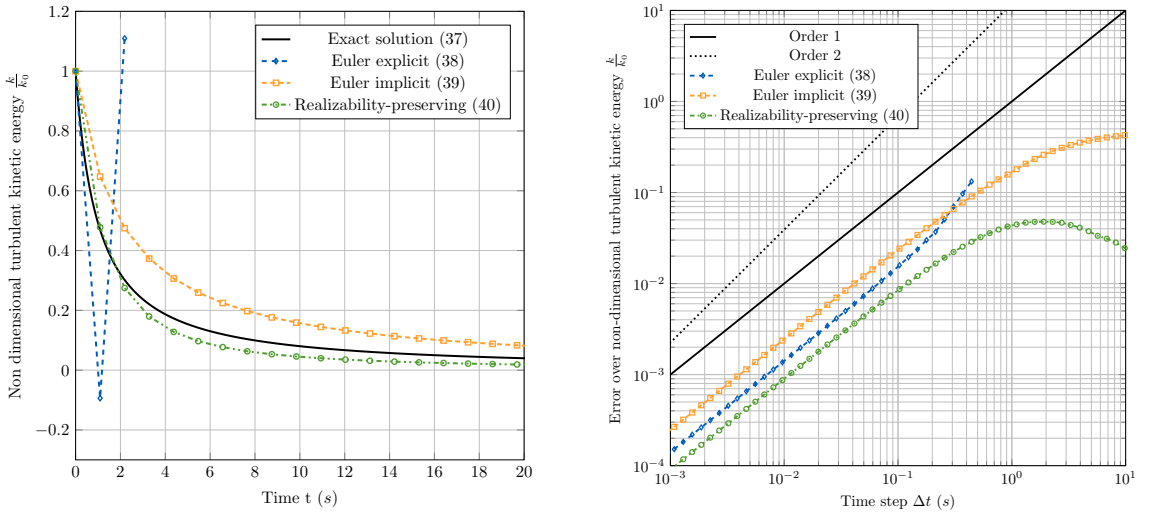


(a) Evolution of $k$ variable.

(b) Time-convergence analysis for the $k$ variable.

Figure 2: Evolution and time-convergence analysis of $k$ with several numerical schemes.

This illustrates the strategy which is followed in Section 4.4 to design implicit destruction terms (and design explicit production ones), but this concept has to be extended to tensor field and that is the purpose of the decomposition theorem presented in Section 4.3.

*4.3. Time-splitting decomposition theorem*

Basic advection and diffusion schemes, namely implicit Euler time stepping for advection and diffusion, with upwind scheme for advection and two-point flux approximation for diffusion, were shown to preserve realizability of the Reynolds stress tensor in a finite volume context. However, other terms of the DRSMs still need to be accounted for, without violating realizability of the numerical schemes. The proposed decomposition theorem is the key ingredient of the present article to achieve this goal at the discrete level. It is first demonstrated, and then we present the methodology utilized for the time-splitting in implicit and explicit parts.

**Theorem 1.** *Let* $\underline{\underline{Sp}}$ *be a SPD tensor of* $\mathbb{R}^n$ *and* $\underline{\underline{Po}}$ *a positive tensor of* $\mathbb{R}^n$*, i.e.* $\forall\, \underline{x} \in \mathbb{R}^n \setminus \{0\}^n$, $\left\langle \underline{\underline{Po}}\, \underline{x}, \underline{x} \right\rangle > 0$. *Let* $\lambda_{\min}^{Po} = \min\limits_{\underline{x},\, |\underline{x}|=1} \left\langle \underline{\underline{Po}}\, \underline{x}, \underline{x} \right\rangle$ *and* $\alpha$ *be such that* $0 \leq \alpha < \lambda_{\min}^{Po}$. *Then, problem* $\mathcal{P}$*: find* $\underline{\underline{T}}$ *in* $\mathcal{S}\left(\mathbb{R}^n\right)$ *solution of:*

$$\frac{1}{2}\left(\underline{\underline{Po}} \cdot \underline{\underline{T}} + \underline{\underline{T}} \cdot \underline{\underline{Po}}^T\right) - \frac{\alpha}{n}\, tr\left(\underline{\underline{T}}\right) \underline{\underline{I_n}} = \underline{\underline{Sp}} \tag{42}$$

*has a unique solution* $\underline{\underline{T}}$ *which is SPD.*

*Proof.* Let $\underline{\underline{f}}$ be a linear map:

$$\underline{\underline{f}} : \left\{ \begin{array}{rcl} \mathcal{S}\left(\mathbb{R}^n\right) & \longrightarrow & \mathcal{S}\left(\mathbb{R}^n\right) \\ \underline{\underline{T}} & \longmapsto & \frac{1}{2}\left(\underline{\underline{Po}} \cdot \underline{\underline{T}} + \underline{\underline{T}} \cdot \underline{\underline{Po}}^T\right) - \frac{\alpha}{n}\, \mathrm{tr}\left(\underline{\underline{T}}\right) \underline{\underline{I_n}}. \end{array} \right. \tag{43}$$

Given $\mathcal{S}\left(\mathbb{R}^n\right)$ of finite dimension, it is sufficient to show that $\underline{\underline{f}}$ is injective to prove that problem $\mathcal{P}$ has a unique solution. Let $\underline{\underline{T}}$ be in the kernel of $\underline{\underline{f}}$. Let $\lambda_1 \leq \ldots \leq \lambda_n$ be the $n$ eigenvalues of $\underline{\underline{T}}$, with associated right-eigenvectors $\underline{e}_1, \ldots, \underline{e}_n$. Given $\left\langle \underline{\underline{f}}\left(\underline{\underline{T}}\right) \underline{e}_i, \underline{e}_i \right\rangle = \lambda_i \left\langle \underline{\underline{Po}}\, \underline{e}_i, \underline{e}_i \right\rangle - \frac{\alpha}{n} \mathrm{tr} \underline{\underline{T}}$, for all $i$ in $\{1, \ldots, n\}$, one obtains:

$$\underline{\underline{M}} \begin{pmatrix} \lambda_1 \\ \vdots \\ \lambda_n \end{pmatrix} = \begin{pmatrix} 0 \\ \vdots \\ 0 \end{pmatrix}, \tag{44}$$

with $\underline{\underline{M}} = \begin{pmatrix} \left\langle \underline{\underline{Po}}\,\underline{e}_1,\, \underline{e}_1 \right\rangle - \frac{\alpha}{n} & -\frac{\alpha}{n} & \cdots & -\frac{\alpha}{n} \\ -\frac{\alpha}{n} & \left\langle \underline{\underline{Po}}\,\underline{e}_2,\, \underline{e}_2 \right\rangle - \frac{\alpha}{n} & \ddots & \vdots \\ \vdots & \ddots & \ddots & -\frac{\alpha}{n} \\ -\frac{\alpha}{n} & \cdots & -\frac{\alpha}{n} & \left\langle \underline{\underline{Po}}\,\underline{e}_n,\, \underline{e}_n \right\rangle - \frac{\alpha}{n} \end{pmatrix}$.

$\underline{\underline{M}}$ is an M-matrix because $0 \leq \alpha < \lambda_{\min}^{Po}$, so $\underline{\underline{M}}$ is invertible: we deduce that $\lambda_1 = \ldots = \lambda_n = 0$ and $f$ is injective. Let now $\underline{\underline{T}}$ be the solution of $\mathcal{P}$. Considering again $\left\langle \underline{\underline{f}}\left(\underline{\underline{T}}\right) \underline{e}_i,\, \underline{e}_i \right\rangle$, for all $i$ in $\{1, \ldots, n\}$, one gets:

$$\underline{\underline{M}} \begin{pmatrix} \lambda_1 \\ \vdots \\ \lambda_n \end{pmatrix} = \begin{pmatrix} \left\langle \underline{\underline{Sp}}\,\underline{e}_1,\, \underline{e}_1 \right\rangle \\ \vdots \\ \left\langle \underline{\underline{Sp}}\,\underline{e}_n,\, \underline{e}_n \right\rangle \end{pmatrix}. \tag{45}$$

$\underline{\underline{M}}$ is an M-matrix, so the inverse is positive (all the components are positive) and one deduces that $\lambda_i > 0$ for all $i$ in $\{1, \ldots, n\}$. □

*4.4. Splitting in time of the DRSM terms*

Realizability preserving time-splitting for the source terms of DRSM are presented in this section. Since advection diffusion of the DRSM preserves realizability with the upwind/implicit finite volume scheme and fulfills decomposition presented in Section 4.3, realizability of the numerical scheme relies on a consistent time-splitting of the model terms. A sufficient condition for the numerical scheme to preserve realizability is for $\underline{\underline{P}} + \underline{\underline{\Phi}} - \underline{\underline{\varepsilon}}$ to admit decomposition (42). Actually, a more restrictive sufficient condition, and easier in practice to derive, is for each of the model terms to verify the decomposition independently. Indeed, by summing up all the contributions:

$$\frac{1}{2}\left(\left(\sum_i \underline{\underline{Po}}_i\right) \cdot \underline{\underline{T}} + \underline{\underline{T}} \cdot \left(\sum_i \underline{\underline{Po}}_i^T\right)\right) - \left(\sum_i \frac{\alpha_i}{3}\right) \mathrm{tr}\left(\underline{\underline{T}}\right) \underline{\underline{1}} = \sum_i \underline{\underline{Sp}}_i, \tag{46}$$

with $\underline{\underline{Po}}_i$, $\underline{\underline{Sp}}_i$ positive and symmetric positive tensors of decomposition (42) applied to each term $i \in \{P, \varepsilon, \phi_r, \phi_s, ...\}$. The sum of SPD matrices being SPD and the sum of positive matrices being positive, decomposition theorem 1 is applied to (46). Hence, provided tensor $\underline{\underline{R}}^n$ is realizable and a decomposition for each of the RHS

term separately, there is a unique $\underline{\underline{T}} = \underline{\underline{R}}^{n+1}$, solution of (46), and this solution is SPD. Which means that the resulting numerical scheme preserves the realizability of the discrete solution. Let us remark that the strict condition $\alpha_i < \lambda_{min}^{Po}$ can be alievated with $\alpha_i \leq \lambda_{min}^{Po_i}$, as long as it is verified by one of the RHS term.

This second approach is used in order to provide a decomposition of $\underline{\underline{P}} + \underline{\underline{\Phi}} - \underline{\underline{\varepsilon}}$. The decomposition for each term is performed as follows:

*Production.* Let us start with the production term: $\rho\underline{\underline{P}} = -\rho\left(\underline{\underline{\nabla}}\ \underline{\overline{u}} \cdot \underline{\underline{R}} + \underline{\underline{R}} \cdot \underline{\underline{\nabla}}\ \underline{\overline{u}}^T\right)$. The velocity gradient can be decomposed as: $\underline{\underline{\nabla}}\ \underline{u}^n = \left(\underline{\underline{\Omega}}^n + \lambda^S_{\max}\underline{\underline{1}}\right) + \left(\underline{\underline{S}}^n - \lambda^S_{\max}\underline{\underline{1}}\right)$ with $\lambda^S_{\max}$, the largest eigenvalue of the strain rate tensor $\underline{\underline{S}}^n$. $-\rho\underline{\underline{P}}\big|_n^{n+1}$ admits the following decomposition:

$$\begin{aligned}
\underline{\underline{Po}}_p &= 2\rho\left(\lambda^S_{\max}\underline{\underline{1}} + \underline{\underline{\Omega}}^n\right), \\
\alpha_p &= 0, \\
\underline{\underline{Sp}}_p &= \rho\left[\left(\lambda^S_{\max}\underline{\underline{1}} - \underline{\underline{S}}^n\right) \cdot \underline{\underline{R}}^n + \underline{\underline{R}}^n \cdot \left(\lambda^S_{\max}\underline{\underline{1}} - \underline{\underline{S}}^n\right)\right].
\end{aligned}$$

The production explicit part $\underline{\underline{Sp}}_p$ is symmetric positive definite and the implicitation matrix $\underline{\underline{Po}}_p$ is positive definite. This decomposition may be modified if IP terms: $-C_1\underline{\underline{P}}^D$ are included in the $\underline{\underline{\Phi}}$ model.

*Dissipation.* Concerning the dissipation term $\rho\underline{\underline{\varepsilon}} = 2\overline{\mu\underline{\underline{\nabla}}\ \underline{u}' \cdot \underline{\underline{\nabla}}\ \underline{u}'^T}$, since the Reynolds stress tensor is invertible. $\rho\underline{\underline{\varepsilon}}\big|_n^{n+1}$ is approximated as:

$$\frac{1}{2}\left(\frac{2}{3}\rho\varepsilon^n\left(\underline{\underline{R}}^n\right)^{-1} \cdot \underline{\underline{R}}^{n+1} + \underline{\underline{R}}^{n+1} \cdot \frac{2}{3}\rho\varepsilon^n\left(\underline{\underline{R}}^n\right)^{-1}\right). \tag{47}$$

Dissipation is fully made implicit with respect to $\underline{\underline{R}}$ by considering the inverse of tensor $\underline{\underline{R}}$ at time-step $n$. This strategy is similar to the one proposed in scheme (40) for the decaying isotropic tubulence with $k-\varepsilon$ model, which is unconditionally realizable. It corresponds to the following decomposition:

$$\begin{aligned}
\underline{\underline{Po}}_\varepsilon &= \frac{2\rho\varepsilon^n}{3}\left(\underline{\underline{R}}^n\right)^{-1}, \\
\alpha_\varepsilon &= 0, \\
\underline{\underline{Sp}}_\varepsilon &= \underline{\underline{0}}.
\end{aligned}$$

*Pressure-strain correlations.* Decomposition is provided for both LRR-IP and SSG models:

**LRR model:** for pressure-strain correlation source terms $\underline{\underline{\Phi}}$ is given by equation (7).

First term $\rho\underline{\underline{\Phi}}_s\Big|_n^{n+1} = -\rho C_1 \frac{\varepsilon}{k}\underline{\underline{R}}^D\Big|_n^{n+1}$ can be fully made implicit:

$$\rho\underline{\underline{\Phi}}_s\Big|_n^{n+1} = -\frac{\rho C_1}{\tau^n}\left(\underline{\underline{R}}^{n+1} - \frac{\mathrm{tr}\left(\underline{\underline{R}}^{n+1}\right)}{3}\underline{\underline{1}}\right), \tag{48}$$

which corresponds to the following decomposition:

$$\begin{aligned}
\underline{\underline{Po}}_{\phi,s} &= \frac{\rho C_1}{\tau^n}\underline{\underline{1}},\\
\alpha_{\phi,s} &= \frac{\rho C_1}{\tau^n},\\
\underline{\underline{Sp}}_{\phi,s} &= \underline{\underline{0}}.
\end{aligned}$$

Second term, corresponding to isotropization of the production term, $\underline{\underline{\Phi}}_r = -C_2\underline{\underline{P}}^D$, is decomposed together with production term $\underline{\underline{P}}$. Since $(1-C_2) > 0$, $\rho(\underline{\underline{P}} + \underline{\underline{\Phi}}_r)\Big|_n^{n+1}$ admits similar decomposition as production:

$$\begin{aligned}
\underline{\underline{Po}}_{\phi,r} &= 2\rho\left(1-C_2\right)\left(\lambda^S_{\max}\underline{\underline{1}} + \underline{\underline{\Omega}}^n\right) - \frac{2\rho C_2}{3}\min\left(P^n, 0\right)\left(\underline{\underline{R}}^n\right)^{-1},\\
\alpha_{\phi,r} &= 0,\\
\underline{\underline{Sp}}_{\phi,r} &= \rho\left(1-C_2\right)\left[\left(\lambda^S_{\max}\underline{\underline{1}} - \underline{\underline{S}}^n\right)\cdot\underline{\underline{R}}^n + \underline{\underline{R}}^n\cdot\left(\lambda^S_{\max}\underline{\underline{1}} - \underline{\underline{S}}^n\right)\right] + \frac{2\rho C_2}{3}\max\left(P^n, 0\right)\underline{\underline{1}}.
\end{aligned}$$

**SSG model:** for the pressure-strain correlation source term $\underline{\underline{\Phi}}$ is provided by equation (8).

Terms $\rho\left(\underline{\underline{\phi}}_{s,1} + \underline{\underline{\phi}}_{r,1}\right)\Big|_n^{n+1} = -\rho\left(C_{s,1}\frac{\varepsilon}{k}\underline{\underline{R}}^D + C_{r,1}\frac{P}{k}\underline{\underline{R}}^D\right)\Big|_n^{n+1}$ are decomposed

altogether:

$$\begin{aligned}
\underline{\underline{Po}}_{\phi,1} &= \frac{\rho}{\tau^n}\max\left(C_{s,1}+C_{r,1}P^{\star n},0\right)\underline{1} - \frac{\rho\varepsilon^n}{3}\min\left(C_{s,1}+C_{r,1}P^{\star n},0\right)\left(\underline{\underline{R}}^n\right)^{-1},\\
\alpha_{\phi,1} &= \frac{\rho}{\tau^n}\max\left(C_{s,1}+C_{r,1}P^{\star n},0\right),\\
\underline{\underline{Sp}}_{\phi,1} &= -\frac{\rho}{\tau^n}\min\left(C_{s,1}+C_{r,1}P^{\star n},0\right)\underline{\underline{R}}^n,
\end{aligned}$$

with $P^{\star n} = \dfrac{tr(\underline{\underline{P}}^n)}{\varepsilon^n}$ .

Term $\rho\underline{\underline{\phi}}_{s,2}\Big|_n^{n+1} = C_{s,2}\rho\dfrac{\varepsilon}{k^2}\left(\underline{\underline{R}}^D\cdot\underline{\underline{R}}^D - \frac{1}{3}\mathrm{tr}(\underline{\underline{R}}^D\cdot\underline{\underline{R}}^D)\underline{1}\right)\Big|_n^{n+1}$:

$$\begin{aligned}
\underline{\underline{Po}}_{\phi,s,2} &= C_{s,2}\frac{\rho}{3\tau^n k^n}\mathrm{tr}(\underline{\underline{R}}^{nD}\cdot\underline{\underline{R}}^{nD})\left(\underline{\underline{R}}^n\right)^{-1},\\
\alpha_{\phi,s,2} &= 0,\\
\underline{\underline{Sp}}_{\phi,s,2} &= C_{s,2}\rho\frac{1}{\tau^n k^n}\left(\underline{\underline{R}}^{nD}\cdot\underline{\underline{R}}^{nD}\right).
\end{aligned}$$

Term $\rho\underline{\underline{\phi}}_{r,2}\Big|_n^{n+1} = \rho\left(C_{r,2} - \dfrac{C_{r,3}}{k}\sqrt{\mathrm{tr}(\underline{\underline{R}}^D\cdot\underline{\underline{R}}^D)}\right)k\underline{\underline{S}}\Big|_n^{n+1}$:

$$\begin{aligned}
\underline{\underline{Po}}_{\phi,r,2} &= |\rho\left(C_{r,2} - \frac{C_{r,3}}{k}\sqrt{\mathrm{tr}(\underline{\underline{R}}^{nD}\cdot\underline{\underline{R}}^{nD})}\right)|k\lambda^S_{\max}\left(\underline{\underline{R}}^n\right)^{-1},\\
\alpha_{\phi,r,2} &= 0,\\
\underline{\underline{Sp}}_{\phi,r,2} &= \rho\left(C_{r,2} - \frac{C_{r,3}}{k}\sqrt{\mathrm{tr}(\underline{\underline{R}}^{nD}\cdot\underline{\underline{R}}^{nD})}\right)k\underline{\underline{S}}\\
&\quad + |\rho\left(C_{r,2} - \frac{C_{r,3}}{k}\sqrt{\mathrm{tr}(\underline{\underline{R}}^{nD}\cdot\underline{\underline{R}}^{nD})}\right)|k\lambda^S_{\max}\underline{\underline{1}}.
\end{aligned}$$

$$\text{Term } \rho\underline{\underline{\phi}}_{=r,3}\Big|_n^{n+1} = \rho C_{r,4}\left(\underline{\underline{R}}^D\cdot\underline{\underline{S}}+\underline{\underline{S}}\cdot\underline{\underline{R}}^D-\frac{2}{3}\mathrm{tr}(\underline{\underline{R}}^D\cdot\underline{\underline{S}})\underline{\underline{1}}\right)\Big|_n^{n+1}:$$

$$\begin{aligned}
\underline{\underline{Po}}_{\phi,r,3} &= \rho\frac{2}{3}C_{r,4}\max\left(\mathrm{tr}(\underline{\underline{R}}^{nD}\cdot\underline{\underline{S}}^n),0\right)\left(\underline{\underline{R}}^n\right)^{-1}\\
&\quad+\rho\frac{4}{3}C_{r,4}k^n\lambda^S_{\max}\left(\underline{\underline{R}}^n\right)^{-1}+2\rho C_{r,4}\lambda^S_{\max}\underline{\underline{1}},\\
\alpha_{\phi,r,3} &= 0,\\
\underline{\underline{Sp}}_{\phi,r,3} &= \rho\frac{2}{3}C_{r,4}\min\left(\mathrm{tr}\left(\underline{\underline{R}}^{nD}\cdot\underline{\underline{S}}^n\right),0\right)\underline{\underline{1}}+\rho\frac{4}{3}C_{r,4}k^n\left(\lambda^S_{\max}\underline{\underline{1}}-\underline{\underline{S}}^n\right)\\
&\quad+C_{r,4}\rho\left[\underline{\underline{R}}^n\cdot\left(\underline{\underline{S}}^n+\lambda^S_{\max}\underline{\underline{1}}\right)+\left(\underline{\underline{S}}^n+\lambda^S_{\max}\underline{\underline{1}}\right)\cdot\underline{\underline{R}}^n\right]
\end{aligned}$$

$$\text{Term } \rho\underline{\underline{\phi}}_{=r,4}\Big|_n^{n+1} = \rho C_{r,5}\left(\underline{\underline{\Omega}}\cdot\underline{\underline{R}}-\underline{\underline{R}}\cdot\underline{\underline{\Omega}}\right)\Big|_n^{n+1}:$$

$$\begin{aligned}
\underline{\underline{Po}}_{\phi,r,4} &= 2\rho C_{r,5}\lambda^S_{\max}\underline{\underline{1}},\\
\alpha_{\phi,r,4} &= 0,\\
\underline{\underline{Sp}}_{\phi,r,4} &= \rho C_{r,5}\left[\left(\underline{\underline{\Omega}}^n+\lambda^S_{\max}\underline{\underline{1}}\right)\cdot\underline{\underline{R}}^n+\underline{\underline{R}}^n\cdot\left(\lambda^S_{\max}\underline{\underline{1}}-\underline{\underline{\Omega}}^n\right)\right].
\end{aligned}$$

Additional RHS terms arising from additional physics such as a buoyancy [5] or

[5]The production by buoyancy effects (weakly-compressible flows) admits a decomposition depending on the stability of the thermal stratification as follows:

$$\begin{aligned}
\rho\underline{\underline{G}}\big|_n^{n+1} &= -\rho\beta_0\frac{3C_\mu}{2\sigma_t}\tau^n\left[\underline{\underline{R}}^n\cdot\underline{\nabla}\overline{T}^n\otimes\underline{g}+\underline{g}\otimes\underline{\nabla}\overline{T}^n\cdot\underline{\underline{R}}^n\right] \qquad \text{if } \underline{\nabla}\overline{T}\cdot\underline{g}>0\\
&= -\rho\beta_0\frac{3C_\mu}{2\sigma_t}\tau^n\left[\underline{\underline{R}}^{n+1}\cdot\underline{\nabla}\overline{T}^n\otimes\underline{g}+\underline{g}\otimes\underline{\nabla}\overline{T}^n\cdot\underline{\underline{R}}^{n+1}\right] \quad \text{otherwise,}
\end{aligned} \tag{49}$$

where we recall that $\tau^n=\frac{k^n}{\varepsilon^n}$ is the local integral turbulent time-scale.

This corresponds to the following decomposition for $-\rho\underline{\underline{G}}\big|_n^{n+1}$, in the case of unstable stratification (i.e. $\underline{\nabla}\rho\cdot\underline{g}<0$):

$$\underline{\underline{Po}}=\underline{\underline{0}},\ \alpha=0,\ \underline{\underline{Sp}}=-\rho\beta_0\frac{3C_\mu}{2\sigma_t}\tau^n\left[\underline{\underline{R}}^n\cdot\underline{\nabla}\overline{T}^n\otimes\underline{g}+\underline{g}\otimes\underline{\nabla}\overline{T}^n\cdot\underline{\underline{R}}^n\right],$$

and for stable conditions (i.e. $\underline{\nabla}\overline{T}\cdot\underline{g}\le 0$):

$$\underline{\underline{Po}}=\rho\beta_0\frac{3C_\mu}{\sigma_t}\tau^n\underline{g}\otimes\underline{\nabla}\overline{T}^n,\ \alpha=0,\ \underline{\underline{Sp}}=\underline{\underline{0}}.$$

Coriolis forces may be decomposed similarily.

The resulting decomposition yields strictly positive tensors for both explicit and implicit source terms. As a consequence, the resulting time-stepping preserves the realizability of the discrete solution.

*4.5. Realizability of the full system*

We now prove that the time-stepping of terms proposed in Section 4.4 combined with basic spatial discretisation schemes presented in Section 4.1 preserve realizability for all cells for $\underline{\underline{R}}^{n+1}$, assuming that $\forall c \in [1;\ N_{cells}], \underline{\underline{R}}_c^n$ is SPD.

Assembling convection-diffusion matrix (33) and its RHS (34) and the proposed time stepping (46) for all other terms reads for all cells $c \in [1;\ N_{cells}]$:

$$\begin{aligned} &\frac{1}{2}\left(\left(\sum_i \underline{\underline{Po}}_i\right)_c \cdot \underline{\underline{R}}_c^{n+1} + \underline{\underline{R}}_c^{n+1} \cdot \left(\sum_i \underline{\underline{Po}}_i^T\right)_c\right) \\ &- \left(\sum_i \frac{\alpha_i}{3}\right)_c \mathrm{tr}\left(\underline{\underline{R}}_c^{n+1}\right) \underline{\underline{I}}_3 + \sum_{\tilde{c}\in[1;\,N_{cells}]} A_{c\tilde{c}}^n \underline{\underline{R}}_{\tilde{c}}^{n+1} = \underline{\underline{B}}_c^n + \left(\sum_i \underline{\underline{Sp}}_i^n\right)_c, \end{aligned} \tag{50}$$

We recall that $\underline{\underline{A}}$ is a M-matrix (diagonal entries are positive and off diagonal entries are negative) and $\underline{\underline{B}}$ a SPD tensor, as shown in Section 4.1. $\underline{\underline{Po}}$ is a positive definite matrix and $\underline{\underline{Sp}}$ a symmetric positive definite one.

Thus, the numerical system can be solved with a Jacobi linear solver and theorem 1 applies for each sub-iterations $k$ and for all cells $c$:

$$\frac{1}{2}\left(\underline{\underline{Po}} \cdot \underline{\underline{R}}_c^{n+1,k+1} + \underline{\underline{R}}_c^{n+1,k+1} \cdot \underline{\underline{Po}}^T\right) - \frac{\alpha}{3}\mathrm{tr}\left(\underline{\underline{R}}_c^{n+1,k+1}\right) \underline{\underline{I}}_3 = \underline{\underline{Sp}}, \tag{51}$$

with:

$$\begin{aligned}
\underline{\underline{Po}} &= A_{cc}\underline{\underline{I}}_3 + \left(\sum_i \underline{\underline{Po}}_i\right)_c, \\
\alpha &= \left(\sum_i \alpha_i\right)_c, \\
\underline{\underline{Sp}} &= \underline{\underline{B}}^n_c - \sum_{\tilde{c}\in[1;\,N_{cells}],\tilde{c}\neq c} A^n_{c\tilde{c}}\underline{\underline{R}}^{n+1,k}_{\tilde{c}} + \left(\sum_i \underline{\underline{Sp}}^n_i\right)_c.
\end{aligned}$$

As for $\varepsilon$, one can use implicit Euler for material convection and diffusion supplemented by space schemes that ensure positiveness (e.g. upwind scheme for material convection and two-point flux approximation for diffusion (Ferrand et al., 2014)). For production and dissipation terms, one can use the following decomposition similar to what is presented in Section 4.2:

$$\rho\frac{\varepsilon}{k}\left(C_{\epsilon 1}P - C_{\epsilon 2}\varepsilon\right)\Big|_n^{n+1} = \rho\frac{\varepsilon^n}{k^n}\left(\max\left[P^n,\,0\right] + \min\left[\frac{P^n}{\varepsilon^n},\,0\right]\varepsilon^{n+1} - C_{\epsilon 2}\varepsilon^{n+1}\right). \quad (52)$$

## 5. Verification with homogeneous shear flows simulations

The realizability of the turbulent models LRR-IP and SSG is studied for incompressible and stationary homogeneous shear flows, with both legacy explicit Euler time-stepping – which uses a component-segregated resolution of $\underline{\underline{R}}$ – and realizability-preserving time-stepping – which requires a component-coupled resolution – implemented in code_saturne. The so-called legacy resolution uses a basic Euler scheme analogous to the what is considered in Section 4.2 for $k-\varepsilon$ model, and thus is consistent with the continuous solution of the turbulence model even in non-realizable zones. The realizability preserving scheme corresponds to the time-steppping derived with the decomposition provided in Section 4.4. The objective of this verification test case is twofold.

Firstly, convergence of the turbulent quantities toward steady solutions obtained from weak-equilibrium is verified for the LRR-IP model. For both time-discretizations (legacy and realizability preserving), equations (3) and (6) are integrated numerically with respect to variable $\underline{\underline{R}}$ and $\varepsilon$, respectively. This approach is usually followed in CFD solvers when it comes to DRSMs. The anisotropy tensor $\underline{\underline{b}}$, the non-dimensional production $P^\star := \frac{tr(\underline{\underline{P}})}{\varepsilon}$ and the turbulent time-scale $\tau = \frac{k}{\varepsilon}$ are calculated and expected to converge towards the steady analytical solution (55). In a DRSM context,

Pope (1975) established the weak-equilibrium hypothesis corresponding to:

$$\frac{\partial}{\partial t}(\rho\underline{\underline{b}}) + \underline{\underline{\mathrm{div}}}\left(\underline{\underline{b}} \otimes \rho\underline{u}\right) + \underline{\underline{D}}_t(\underline{\underline{b}}) + \underline{\underline{D}}_\nu(\underline{\underline{b}}) + \underline{\underline{D}}_p(\underline{\underline{b}}) = \underline{\underline{0}} \implies \underline{\underline{P}} + \underline{\underline{\Phi}} - \underline{\underline{\varepsilon}} = \underline{\underline{0}} \tag{53}$$

Considering the LRR-IP model with imposed constant shear stress $\underline{\underline{\nabla u}} = S\underline{e}_x \otimes \underline{e}_z$ and homogeneous turbulence, analytical solution of equation (53) writes (see Appendix B for a proof):

$$\underline{\underline{b}} = \begin{pmatrix} \frac{\frac{4}{9}(1-C_2)^2 S^{\star 2}}{(C_1-1+P^\star)^2 + (1-C_2)^2 \frac{2}{3} S^{\star 2}} & 0 & \frac{-\frac{1}{3}(1-C_2)(C_1-1+P^\star) S^\star}{(C_1-1+P^\star)^2 + (1-C_2)^2 \frac{2}{3} S^{\star 2}} \\ 0 & \frac{-\frac{2}{9}(1-C_2)^2 S^{\star 2}}{(C_1-1+P^\star)^2 + (1-C_2)^2 \frac{2}{3} S^{\star 2}} & 0 \\ \frac{-\frac{1}{3}(1-C_2)(C_1-1+P^\star) S^\star}{(C_1-1+P^\star)^2 + (1-C_2)^2 \frac{2}{3} S^{\star 2}} & 0 & \frac{-\frac{2}{9}(1-C_2)^2 S^{\star 2}}{(C_1-1+P^\star)^2 + (1-C_2)^2 \frac{2}{3} S^{\star 2}} \end{pmatrix}, \tag{54}$$

with:

$$S^\star = \tau S, \qquad P^\star = \frac{C_{\varepsilon 2} - 1}{C_{\varepsilon 1} - 1}, \qquad \tau = \frac{\sqrt{3}}{\sqrt{2}} \frac{|C_1 - 1 + P^\star|}{S} \sqrt{\frac{P^\star}{(C_1 - 1 + P^\star C_2)(1 - C_2)}} \tag{55}$$

Secondly, realizability of the trajectories toward the steady algebraic solution of the modelled equations is investigated in an invariant context with both LRR-IP and SSG models. It can be noticed that the steady algebraic solution of the LRR-IP model is realizable.

In this context, both the convection and diffusion operators in equation (3) cancel out by construction. Hence, the solution and its realizability are investigated independently from the convection-diffusion numerical scheme, only unsteady and RHS terms actually play a part.

### *5.1. Numerical setup*

Numerical simulations proposed by Durbin and Speziale (1994) aim at (i) reproducing non-realizable transients towards constant and homogeneous shear stress flows with LRR-IP and SSG models with legacy algorithms (ii) showing that the new-time stepping proposed in Section 4.4 allows to enforce realizability in a weak-equilibrium context (iii) verifying accordance with analytical results. A mesh made of one hexahedron with periodic conditions along longitudinal axes is used to account for homogeneity. A constant unit velocity gradient is imposed in the vertical direction through velocity Dirichlet boundary conditions at the top and bottom faces. This corresponds to constant shear stress in a boundary layer. In order to account

for homogeneity of turbulence, homogeneous Neumann boundary conditions are imposed in the vertical direction for $\underline{\underline{R}}$ and $\varepsilon$ equations. Runtime is taken as a few turbulent integral characteristic time-scales $\tau$. Since resolved variables $\underline{\underline{R}}$ and $\varepsilon$ keep increasing in magnitude because of the constant shear stress, computational runtime is limited by the computer's arithmetic since the magnitude of $\underline{\underline{R}}$ keeps increasing during the simulation, while the turbulent anisotropy tensor gets steady.

*5.2. Numerical results*

*LRR-IP model.* Two-sets of realizable initial conditions (presented in Table 4) have been used with LRR-IP model. First of all, numerical $P^\star$ and characteristic time $\tau$ are compared to the analytical ones. Numerical results are presented in Figures 3 and 4 for $P^\star$ and $\tau$, respectively. Sufficient realizability condition $P^\star \geq -\frac{4}{3}$ (Durbin and Speziale, 1994), obtained from both the strong form of realizability and stochastic considerations (see section Appendix A.2), is not fulfilled. Then, convergence of the

| | $S$ ($s^{-1}$) | $k$ ($m^2s^{-2}$) | $S^\star$ | $b_{11}$ | $b_{22}$ | $b_{33}$ | $b_{12}$ | $b_{13}$ | $b_{23}$ | $P^\star$ | $-I_2$ | $I_3$ |
|---|---|---|---|---|---|---|---|---|---|---|---|---|
| Set 1 | 1.0 | 0.0006 | 3.0 | 0.16 | -0.32 | 0.16 | 0 | 0.4 | 0 | -1.2 | 0.0563 | 0.0043 |
| Set 2 | 1.0 | 0.0006 | 10 | 0.15 | -0.3 | 0.15 | 0 | 0.3 | 0 | -3.0 | 0.158 | 0.020 |

Table 4: Realizable initial conditions from (Durbin and Speziale, 1994) - LRR-IP model.

non-zero components of the anisotropy tensor $\underline{\underline{b}}$ toward analytical stationary solutions are presented in Figures 8 and 9. $b_{ij}^{LRR}$ and $b_{ij}^{ALGE}$ stand for the $(i^{th}, j^{th})$ component of the anisotropy tensor predicted with realizable LRR-IP numerical scheme and the algebraic solution, respectively. Numerical results are in accordance with the analytical results and the relative errors keep decreasing with respect to $S \times t$, the non-dimensional time.

As a second step, realizability of the trajectories toward stationary solutions are studied. Trajectories in the ($\xi$, $\eta$) plane with both realizability preserving time-stepping and the legacy solver's time-stepping, departing from the first and the second set of initial conditions are presented in Figure 5 and 6, respectively. For the solutions to be realizable, the invariants have to remain inside the Lumley's triangle. Numerical results obtained with the legacy resolution are in accordance with the ones presented in Durbin and Speziale (1994) and break realizability. However, the new time-stepping allows to enforce realizability of the Reynolds stress tensor during the simulation. Furthermore, sufficient condition $P^\star \geq -\frac{4}{3}$ is shown to be too restrictive since it is not fulfilled with the coupled resolution, while realizability is preserved.

*SSG model.* Analytical solution for the anisotropy tensor with the SSG model is not presented in the present work. Realizability of the trajectories in the plane ($\xi$, $\eta$) were studied departing from initial conditions presented in Table 5.

| $S$ ($s^{-1}$) | $k$ ($m^2s^{-2}$) | $S^\star$ | $b_{11}$ | $b_{22}$ | $b_{33}$ | $b_{12}$ | $b_{13}$ | $b_{23}$ | $P^\star$ | $-I_2$ | $I_3$ |
|---|---|---|---|---|---|---|---|---|---|---|---|
| 1.0 | 0.0006 | 20 | -0.27 | 0.6 | -0.33 | 0 | 0 | 0 | 0 | 0.27 | 0.053 |

Table 5: Realizable initial conditions for turbulent structures from Durbin and Speziale (1994) using SSG model.

Numerical results obtained with both legacy and realizability-preserving time-steppings of the SSG model are presented in Figure 7. Similarly to LRR-IP model, while the legacy time-stepping produces unrealizable trajectories, the new one allows to enforce realizability of the Reynolds stress tensor during the simulation.

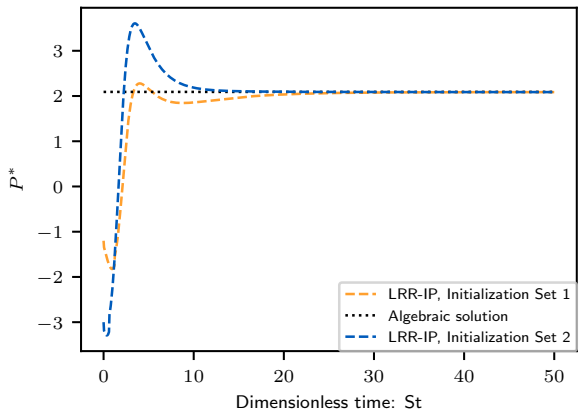


Figure 3: Homogeneous shear flow simulations with LRR-IP model and initial conditions from Table 4. Non-dimensional turbulent production rate $P^*$ with respect to dimensionless time.

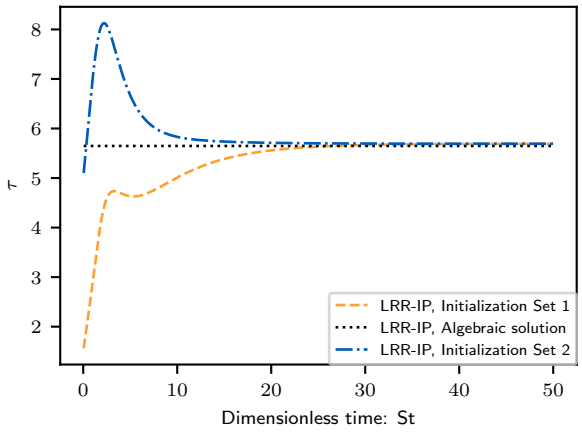


Figure 4: Homogeneous shear flow simulations with LRR-IP model and initial conditions from Table 4. Turbulent time-scale $\tau$ with respect to dimensionless time.

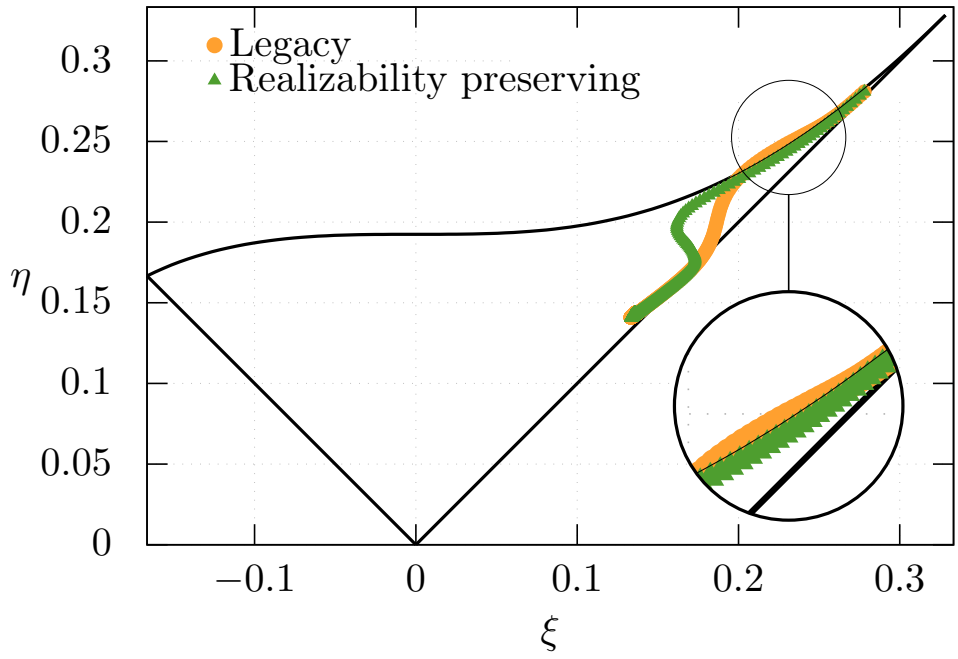


Figure 5: Anisotropy invariants in Lumley's triangle for the homogeneous shear flow simulation with LRR-IP model and initial conditions from set 1 in Table 4 (upper-right corner of the triangle).

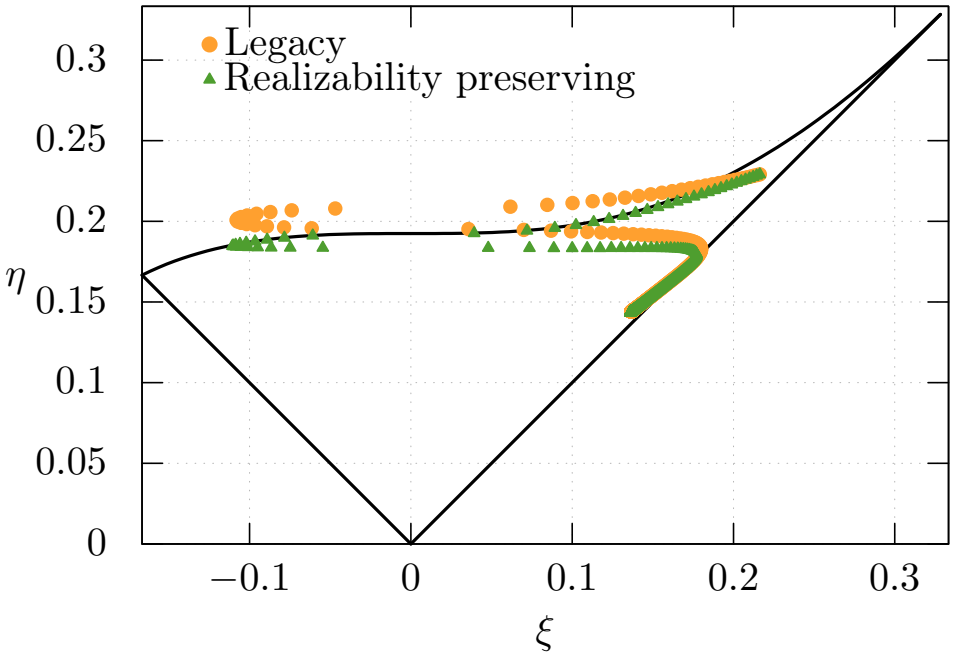


Figure 6: Anisotropy invariants in Lumley's triangle for the homogeneous shear flow simulation with LRR-IP model and initial conditions from set 2 in Table 4 (upper-right corner of the triangle).

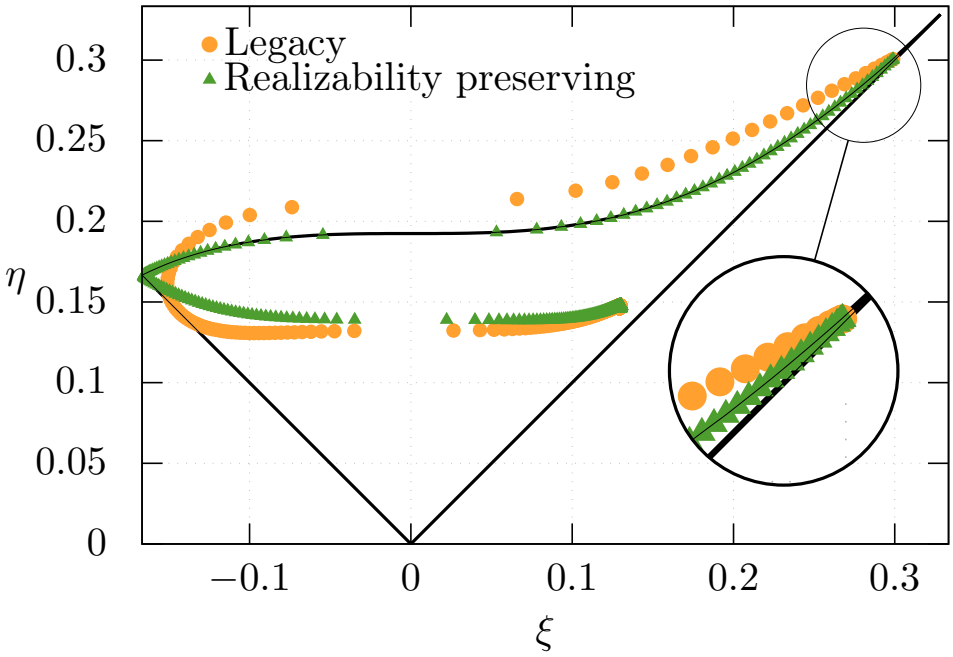


Figure 7: Anisotropy invariants in Lumley's triangle for the homogeneous shear flow simulation with SSG model and initial conditions from Table 5 (upper-right corner of the triangle).

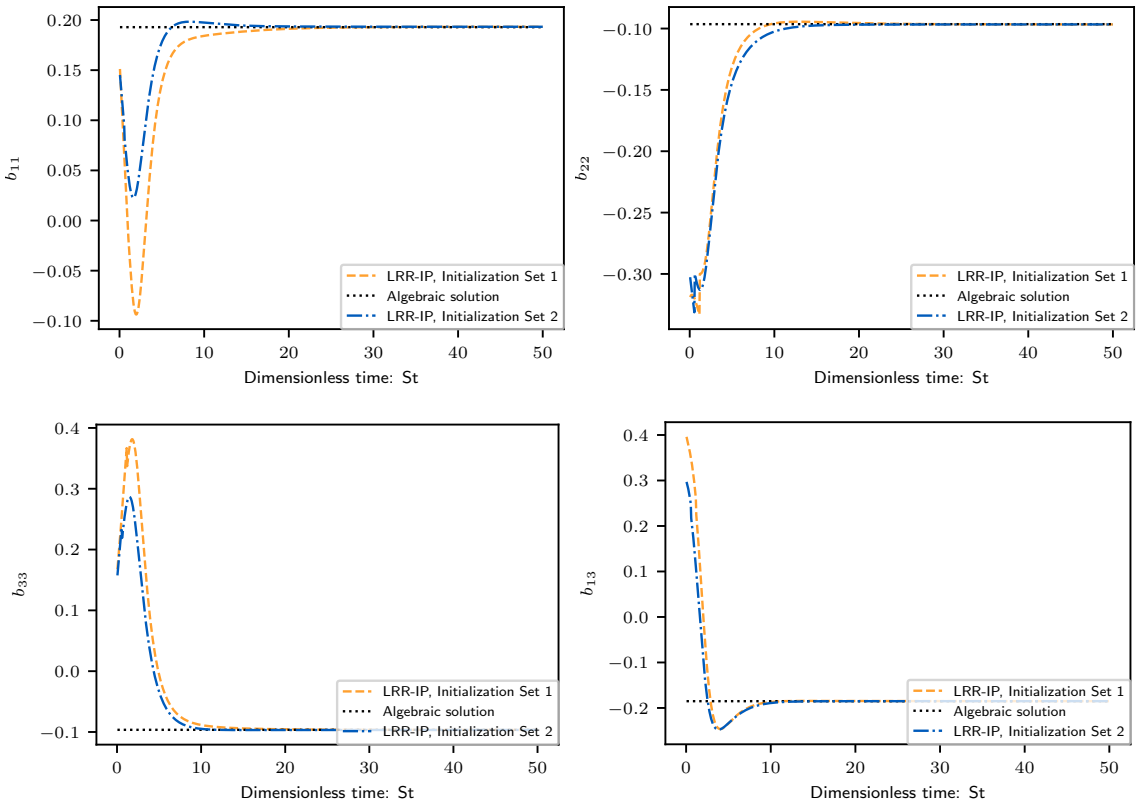


Figure 8: Homogeneous shear flow simulations with LRR-IP model - Anisotropy tensor components with respect to time.

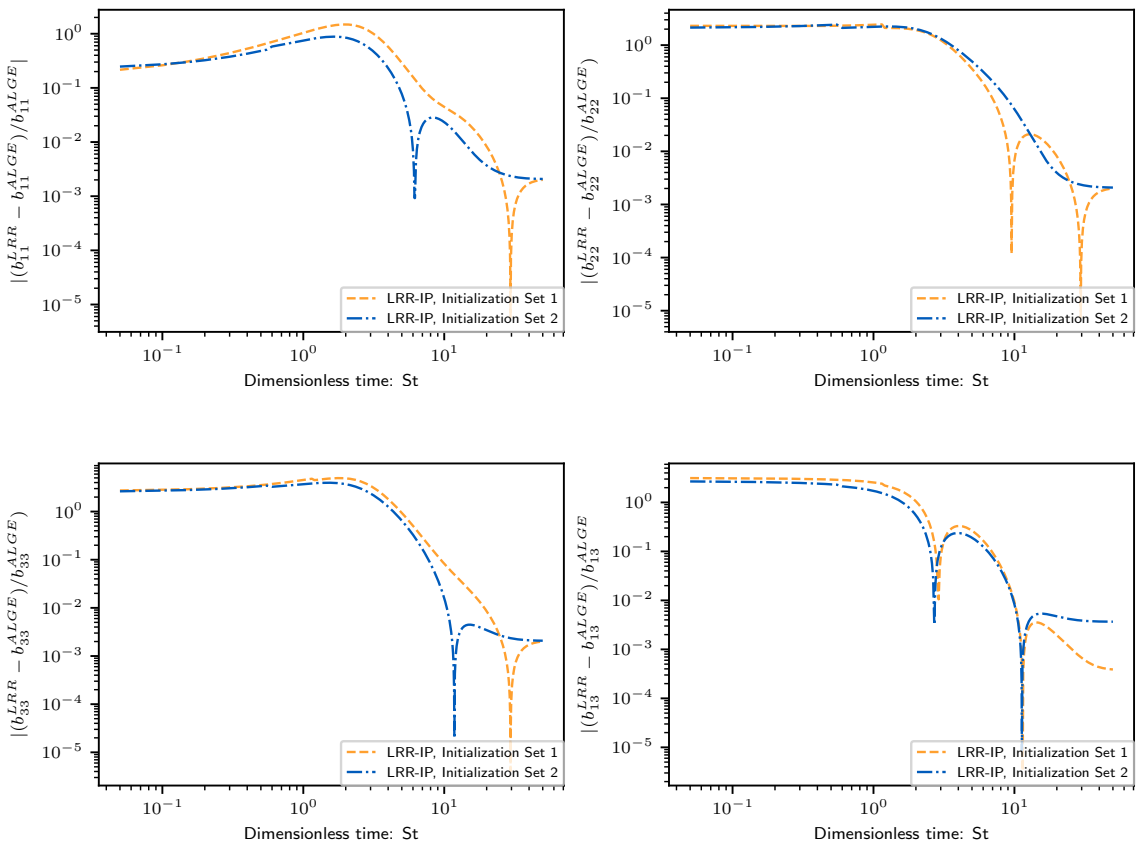


Figure 9: Homogeneous shear flow simulations with LRR-IP model - Anisotropy tensor relative error to algebraic steady solution with respect to time.

## 6. Illustration of practical benefits of the realizability preserving time-stepping on a turbulent flow in a cylindrical pipe with a U-bend

The aim of this section is to illustrate some practical benefits of using a realizability preserving time-stepping compared to standard numerical clipping of the Reynolds stresses.

### *6.1. Case Description*

The turbulent flow through a U-bend 3D configuration is computed by a CFD computation using code_saturne and compared with experimental reference data provided by Azzola et al. (1986). They investigated both experimentally and numerically the developing turbulent flow in a strongly curved 180° pipe bend. The velocity profiles are measured at several cross sections as depicted in Figure 10.

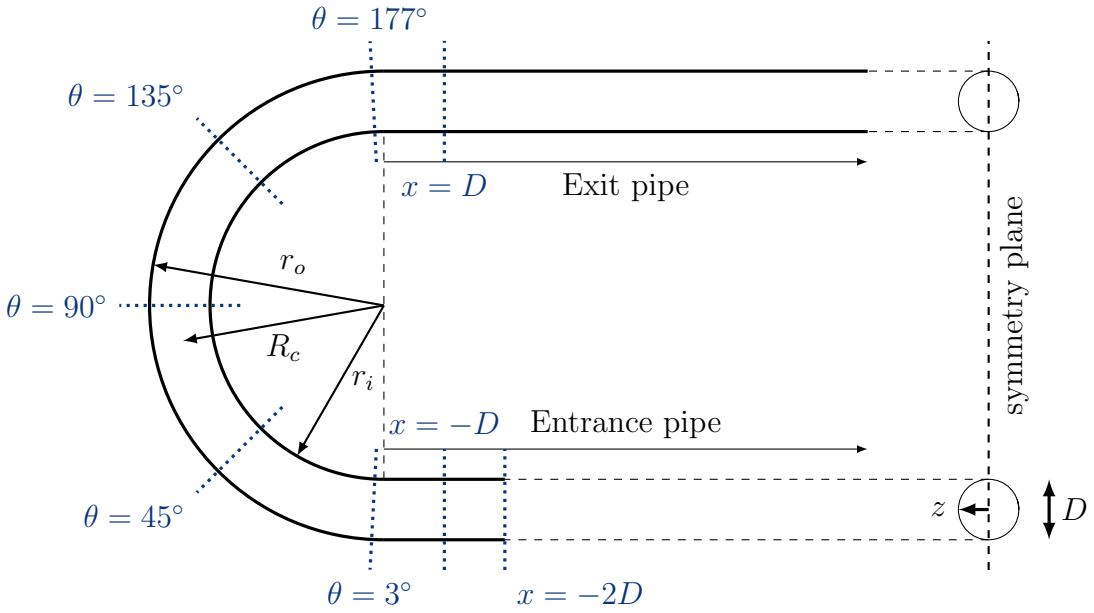


Figure 10: Sketch of the experimental configuration.

The U-bend cross section is circular throughout with a diameter $D = 0.0445\,\mathrm{m}$ and the ratio between the bend mean radius and the curvature to pipe diameter is $R_c/D = 3.375$. Both tangents are experimentally of length $L_x = 54.7\ D$, being respectively attached to the 0° (inlet) and 180° (outlet) planes of the bend by means of flanges.

We refer to Azzola et al. (1986) experiment for the bulk average velocity value corresponding to $U_b = 1.29\,\mathrm{m/s}$. Values for the Reynolds numbers based on physical properties of water at 20° C is $Re = 57\ 400$ and the associated Dean number $De = \sqrt{D/(2R_c)}\ \rho D U_b/\mu = 31\ 300$.

The measurements of the stream-wise velocity component at different sections are performed for $x/D = -2,\ -1,\ 1,\ 2,\ 3,\ 4$ and 5 in the straight pipes and $\theta = 3°,\ 45°,\ 90°,\ 135°$ and $177°$ in the bend. At each of these sections 15 radial positions are probed, starting from the centre-line and moving to the wall with an increment of 1.5 mm toward the wall.

*6.2. CFD data setting*

The 3D CFD domain was generated and meshed using SALOME and is shown in Figure 11. The straight pipe is $2 \times D$ long at the inlet and $8 \times D$ long at the outlet. The mesh is composed of 295 680 hexahedral cells (see Figure11) with the near wall cell size of $(\Delta y)_1 = 1.5\,\mathrm{mm}$ which gives $y_w^+ \coloneqq \dfrac{\rho y u_\star}{\mu} \in [20;\ 60]$.

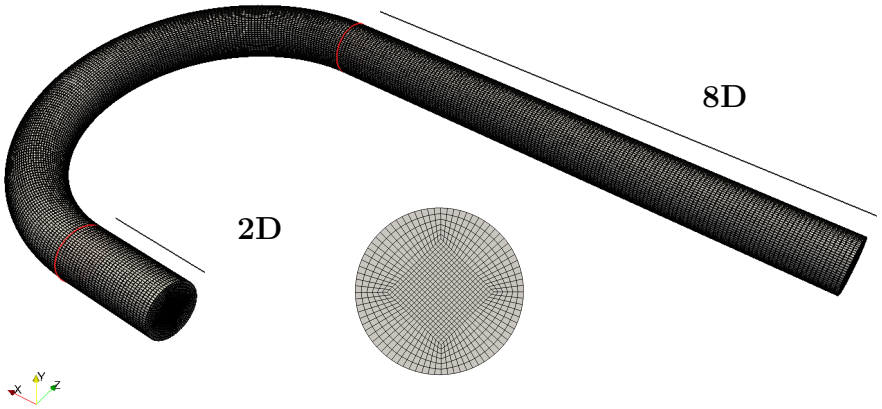


Figure 11: View of the 3D hexahedral mesh.

The CFD calculations are performed with code_saturne version 8.0.

The fluid density is considered as constant with $\rho = 1 \times 10^3\,\mathrm{kg\ m^{-3}}$, the dynamic viscosity is set to $\mu = \frac{\rho D U_b}{Re}$ and the bulk velocity is set to $U_b = 1\,\mathrm{m\,s^{-1}}$ so that the Reynolds number is $Re \coloneqq \frac{\rho U_b D}{\mu} = 57\ 400$. At the inlet, the following normal velocity

component profile is imposed (obtained using a polynomial fit of the experimental data):

$$\frac{u\left(r^{+}\right)}{U_b} = 1.162 + 0.025 \times r^{+} - 0.871 \times (r^{+})^2 - 1.197 \times (r^{+})^3, \tag{56}$$

with $r^{+} \coloneqq \frac{r}{D}$, the other components are set to zero. At the outlet, default free outlet boundary conditions are used.

The $R_{ij}-\varepsilon$ SSG turbulence model is used with both the segregated legacy and the realizability-preserving time-steppings with two velocity scales standard wall function.

For all runs, the material convection schemes set by default in code_saturne v8.0 are used, namely a second order centered scheme for the velocity with slope tests enabled and an upwind scheme for the Reynolds stress tensor and $\varepsilon$. Gradients are computed using the Green-Gauss iterative algorithm. Linear solvers for all transported quantities is Jacobi with a relative precision of $10^{-8}$.

### *6.3. Results*

The streamwise velocity steady state results for both algorithms are very similar as shown in Figure 12. However, in the transient we notice that the number of clippings needed are kept to 0 with the realizability-preserving scheme, while it is not the case with the legacy segregated solver (see Figure 13(a)). The new scheme improves drastically the linear solver resolution compared to the legacy scheme (roughly a factor 2 is obtained for the number of inner-iterations) during the transient as displayed in Figure 13(b). These results show that the algorithm presented in this article, in addition to ensure a positive definite Reynolds stress tensor at all time steps, increases the robustness and may decrease the CPU needed to inverse the linear system (the results when reaching a steady state are sensibly the same).

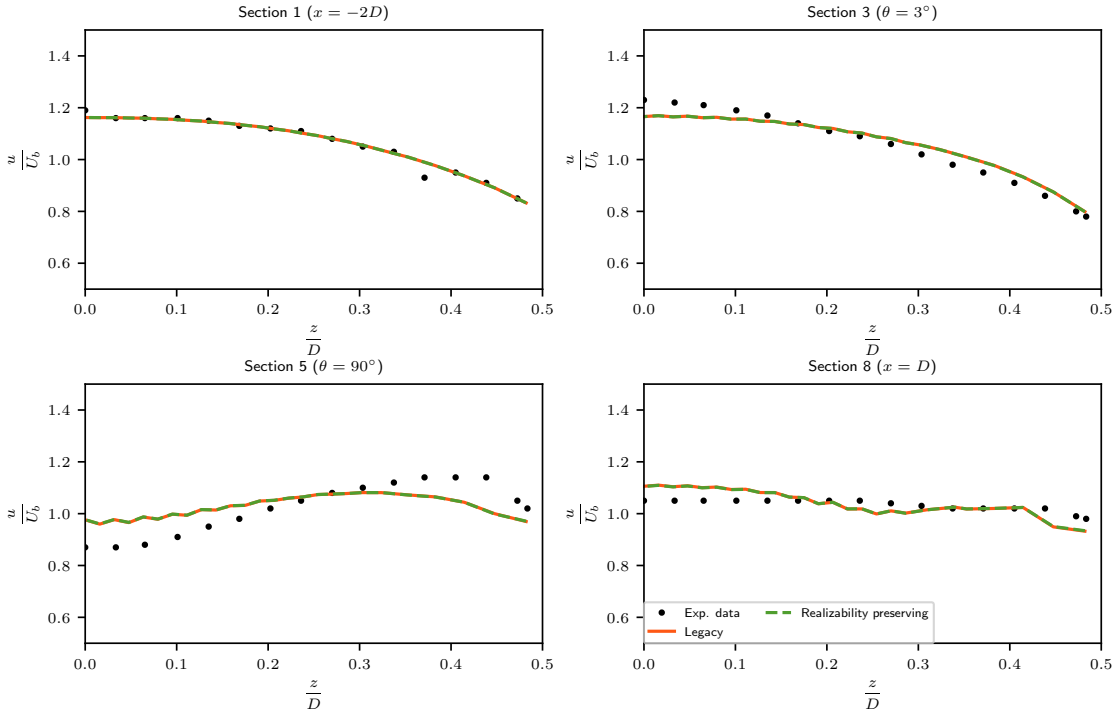


Figure 12: Stream-wise velocity profiles at sections 1 to 8 for the legacy algorithm and the realizability preserving time-stepping.

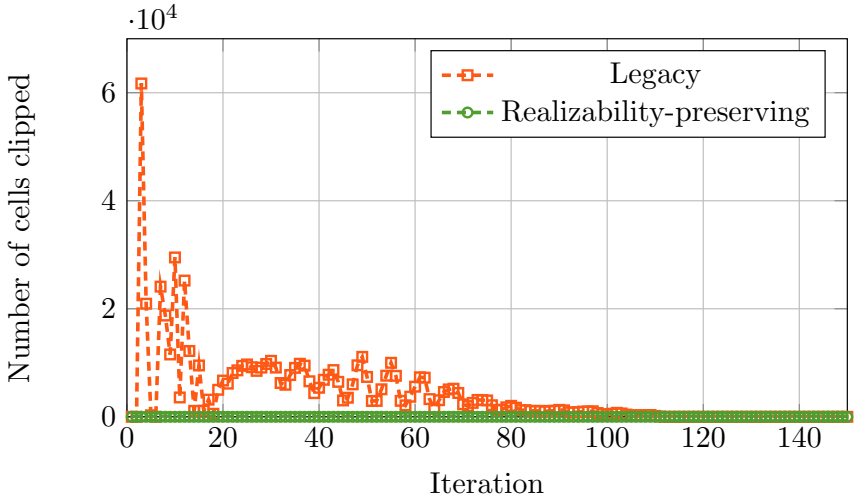


(a) Number of cells with $\underline{\underline{R}}$ clipped.

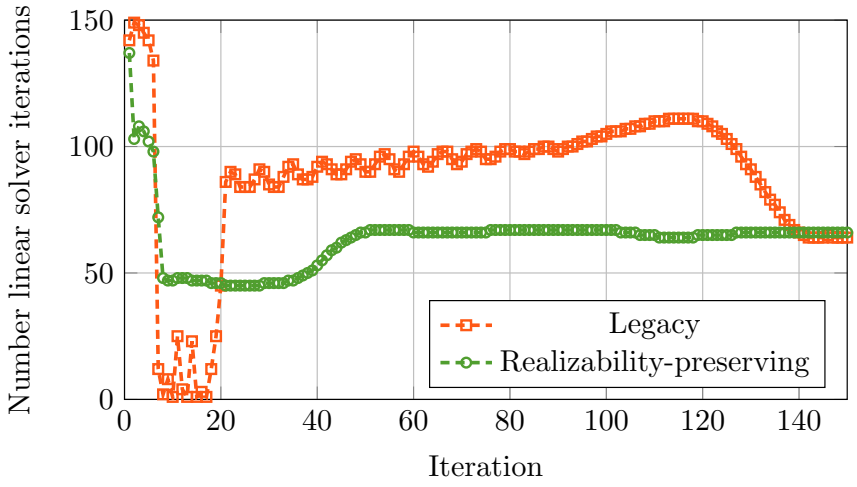


(b) Linear solver efficiency.

Figure 13: Comparison of the number of clipped cells for each component of $\underline{\underline{R}}$ with both the realizability-preserving and the legacy solvers for U-bend test case using the SSG model. The total number of cells is $\approx$ 110 000. For the coupled solver there is no clipping at all for any of the components. This induces improvements in the linear solver resolution during the transient.

## 7. Conclusion

Second moment closure turbulence models should verify realizability criteria. This is a warranty for both physical reliability and robustness of the numerical solvers. While several models such as LRR-IP and SSG were shown to break realizability, methods to preserve this property at continuous level were proposed by several authors. However, realizability at continuous level does not guarantee that same property holds for the discretized equations, which depends on the numerical schemes at stake. In this context, another approach relying on realizability preserving numerical scheme is proposed. Provided realizability-preserving convection and diffusion discrete operators for the Reynolds stress tensor transport equation, which were proposed in the present article for a basic finite volume scheme, realizability conservation relies on the discretization of the right-hand-side terms. Hence, time-splitting allowing solution tensor field to remain symmetric semi-positive definite, is sufficient for ensuring realizability of the Reynolds stress tensor. Provided decomposition theorem, new time-steppings for some models were shown to preserve these criteria analytically. Numerical experiments with shear flows, known in the literature to be responsible for breaking realizability are in accordance with analytical results. Furthermore, analytical exact solutions for homogeneous shear flows were derived in order to investigate accuracy of the numerical scheme, in the context of simplified configurations. Finally, practical numerical benefits of the realizability preserving scheme were highlighted on a turbulent flow in a cylindrical pipe with a U-bend. In this case, the scheme allows avoiding clippings by keeping the Reynolds stress tensor realizable and improves the performances of the solver.

## References


S. B. Pope, Turbulent flows, Cambridge University Press, 2000.

K. Hanjalić, B. Launder, Modelling turbulence in engineering and the environment: second-moment routes to closure, Cambridge university press, 2011.

U. Schumann, Realizability of reynolds-stress turbulence models, The Physics of Fluids 20 (1977) 721–725.

J. L. Lumley, Computational modeling of turbulent flows, Advances in applied mechanics 18 (1979) 123–176.

J. L. Lumley, Turbulence modeling, ASME Journal of Applied Mechanics 50 (1983) 1097–1103.

B. E. Launder, G. J. Reece, W. Rodi, Progress in the development of a reynolds-stress turbulence closure, J. Fluid Mechanics 68 (1975) 537–566.

C. G. Speziale, S. Sarkar, T. B. Gatski, Modelling the pressure strain correlation of turbulence : an invariant dynamical systems approach, J. Fluid Mechanics 227 (1991) 245–272.

T. H. Shih, J. L. Lumley, Modeling of pressure correlation terms in reynolds stress and scalar flux equation, Cornell University Technical Report FDA-85-3 (1985).

T. H. Shih, A. Shabbir, Methods of ensuring realizability for non-realizable second order closures, NASA Technical Memorandum 106681 (1994).

J. W. Deardorff, The use of subgrid transport equations in a three-dimensional model of atmospheric turbulence, ASME J. Fluid Eng. 95 (1973) 429–438.

J. Chassaing, G. Gerolymos, I. Vallet, Efficient and robust reynolds-stress model computation of three-dimensional compressible flows, AIAA journal 41 (2003) 763–773.

Y. Mor-Yossef, Y. Levy, Unconditionally positive implicit procedure for two-equation turbulence models: application to k-$\omega$ turbulence models, Journal of Computational Physics 220 (2006) 88–108.

Y. Mor-Yossef, Y. Levy, The unconditionally positive-convergent implicit time integration scheme for two-equation turbulence models: revisited, Computers & fluids 38 (2009) 1984–1994.

Y. Mor-Yossef, Unconditionally stable time marching scheme for reynolds stress models, Journal of Computational Physics 276 (2014) 635–664.

EDF, code_saturne software, 2023. URL: `http://www.code-saturne.org`.

F. Dehoux, S. Benhamadouche, R. Manceau, An elliptic blending differential flux model for natural, mixed and forced convection, International Journal of Heat and Fluid Flow, Elsevier 63 (2017) 190–204.

G. Mangeon, S. Benhamadouche, J.-F. Wald, R. Manceau, Extension to various thermal boundary conditions of the elliptic blending model for the turbulent heat flux and the temperature variance, Journal of Fluid Mechanics 905 (2020) A1.

M. L. Bahlali, C. Henry, B. Carissimo, On the well-mixed condition and consistency issues in hybrid eulerian/lagrangian stochastic models of dispersion, Boundary-Layer Meteorology 174 (2020) 275–296.

G. Balvet, J.-P. Minier, C. Henry, Y. Roustan, M. Ferrand, A time-step-robust algorithm to compute particle trajectories in 3-d unstructured meshes for lagrangian stochastic methods, Monte Carlo Methods and Applications (2023).

H. Amino, C. Flageul, S. Benhamadouche, I. Tiselj, B. Carissimo, M. Ferrand, A time-staggered second order conservative time scheme for variable density flow, International Journal for Numerical Methods in Fluids 94 (2022) 1964–1995.

C. C. Shir, A preliminary numerical study of atmospheric turbulent flows in the idealized planetary boundary layer, Journal of the Atmospheric Sciences 30 (1973) 1327–1339.

J. Rotta, Statistische theorie nichthomogener turbulenz, Z. Physik 129 (1951) 547–572.

D. Naot, A. Shavit, M. Wolfstein, Interactions between components of the turbulent velocity correlation tensor, Israel J. Tech 8 (1970) 259–269.

J. L. Lumley, Computational modeling of turbulent flows, Advances in applied mechanics 18 (1979) 123–176.

M. Ferrand, J. Fontaine, O. Angelini, An anisotropic diffusion finite volume algorithm using a small stencil, in: Finite Volumes for Complex Applications VII-Elliptic, Parabolic and Hyperbolic Problems, volume 78, 2014, pp. 577–585.

B. Mohammadi, O. Pironneau, Analysis of the k-epsilon turbulence model, 1993.

S. B. Pope, A more general effective-viscosity hypothesis, Journal of Fluid Mechanics 72 (1975) 331–340.

P. A. Durbin, C. Speziale, Realizability of second-moment closure via stochastic analysis, Journal of Fluid Mechanics 280 (1994) 395–407.

J. Azzola, J. Humphrey, H. Iacovides, B. Launder, Developing turbulent flow in a u-bend of circular cross-section: Measurement and computation, Transaction of the ASME 108 (1986) 214–221.

C. Speziale, E. Abid, P. Durbin, On the realizability of reynolds stress turbulence closures, Journal of Scientific Computing 9 (1994) 369–403.

S. B. Pope, Pdf methods for turbulent reactive flows, Progress in Energy and Combustion Science 11 (1985) 119–192.

## Appendix A. Realizability of the continuous models

From a modelling standpoint, necessary conditions are utilized to demonstrate non-realizability of several turbulence models and only sufficient conditions are considered by authors in order to design realizable ones Shih and Lumley (1985); Shih and Shabbir (1994). It corresponds to the weak and strong forms of realizability, respectively (see Schumann (1977); Lumley (1979); Speziale et al. (1994)). In that respect, authors considered realizable initial and boundary conditions and assumed some regularity for the trajectories of the turbulent quantities. In the following, $\underline{\underline{R}}$ is assumed to be sufficiently smooth.

### *Appendix A.1. Weak and strong forms of realizability*

*Weak form of realizability (necessary condition).* Let $\alpha$ denotes a principal direction of the Reynolds stress tensor. In principal coordinates, $\underline{\underline{R}}$ is diagonal and the realizability constraint reduces to $R_{\alpha\alpha}$ being non-negative ($\underline{\underline{\mathrm{R}}}$ symmetric semi-positive definite). Necessary conditions for preserving realizability in principal coordinates is:

$$R_{\alpha\alpha} = 0 \Rightarrow \frac{\overline{D}}{\overline{D}t} R_{\alpha\alpha} \geq 0. \tag{A.1}$$

This means that $\underline{\underline{R}}$, should not cross the realizability limit. U. Schumann (1977) assumed more regularity, for $\underline{\underline{R}}$ in $C^1(\mathbb{R}^d, \mathbb{R}^+)^{d\times d}$, total derivative being continuous:

$$R_{\alpha\alpha} = 0 \Rightarrow \frac{\overline{D}}{\overline{D}t} R_{\alpha\alpha} = 0. \tag{A.2}$$

Relation (A.1) is called the weak form of realizability. It is necessary but not sufficient condition for ensuring realizability departing from realizable initial and boundary conditions. Indeed, let us consider at given position and time $(\underline{x}, t)$:

$$R_{\alpha\alpha}(\underline{x}, t) = 0; \frac{\overline{D}}{\overline{D}t} R_{\alpha\alpha}(\underline{x}, t) = 0; \quad \frac{\overline{D}^2}{\overline{D}t^2} R_{\alpha\alpha}(\underline{x}, t) < 0. \tag{A.3}$$

$R_{\alpha\alpha}$ obviously satisfies equation (A.1). For $\underline{\underline{R}}$ sufficiently smooth, one obtains $R_{\alpha,\alpha}(\underline{x}, t) < 0$ in a neighborhood of $(\underline{x}, t)$. Tensor $\underline{\underline{R}}$ is not semi-positive definite anymore and realizability is broken.

*Strong form of realizability (sufficient condition).* Lumley (1979) introduced the strong form of realizability, which includes requirement over second time derivatives of $\underline{\underline{R}}$, whenever $R_{\alpha\alpha}$ cancels in a principal coordinates system:

$$R_{\alpha\alpha} = 0 \Rightarrow \begin{cases} \dfrac{\overline{D}}{\overline{D}t} R_{\alpha\alpha} = 0, & \dfrac{\overline{D}^2}{\overline{D}t^2} R_{\alpha\alpha} > 0. \end{cases} \tag{A.4}$$

Then, Pope (1985) proposed a generalization:

$$\begin{cases} R_{\alpha\alpha} = 0, & \dfrac{\overline{D}^i}{\overline{D}t^i} R_{\alpha\alpha} = 0, \forall i \in \{1, p-1\} \Rightarrow \dfrac{\overline{D}^p}{\overline{D}t^p} R_{\alpha\alpha} > 0, \end{cases} \tag{A.5}$$

with $p \geq 2$ denoting the index of the first non-null total derivative of $\underline{\underline{R}}$.
Another set of sufficient conditions for ensuring realizability of the Reynolds stress tensor is provided in Speziale et al. (1994), based on the "over-realizability" concept introduced by Schumann (1977). By preventing one and two components turbulent states to be reached in finite time, this allows to circumvent difficulty exposed in last subsection by obviating conditions on second order total derivative of $R_{\alpha\alpha}$. Sufficient condition is:

$$R_{\alpha\alpha} = 0 \Rightarrow \frac{\overline{D}}{\overline{D}t} R_{\alpha\alpha} > 0. \tag{A.6}$$

*Appendix A.2. Realizability of the exact and modelled transport equations*

From definitions, the Reynolds stress tensor $\underline{\underline{R}}$ has to fulfill the realizability conditions (15). Hence, one may reasonably expect its unclosed transport equation to achieve realizability at any time and position assuming realizable initial and boundary conditions. Schumann (1977) provides proof of the realizability of the exact transport equation for incompressible fluids, completed by Speziale et al. (1994). Similarly, realizability of the LRR-IP model was investigated at continuous level in an incompressible context. Lumley (1979) argued that linear return to isotropy model cannot be realizable, while several non-linear return to isotropy models were shown to preserve realizability. However, the SSG model, considered in the present work do not preserve it *a priori*. Hereafter, special attention is paid to realizability of the exact transport equations equation and those of the LRR-IP model implemented

in code_saturne. In $\underline{\underline{R}}$ eigenbasis, a DRSM write:

$$\begin{aligned}\left(\frac{\overline{D}}{\overline{D}t}\underline{\underline{R}}\right)_{\alpha\beta} &= \rho\frac{\overline{D}}{\overline{D}t}R_{\alpha\beta} + \rho\frac{\overline{D}}{\overline{D}t}(V_{\alpha i})V_{ki}R_{k\beta} + \rho R_{\alpha i}V_{ik}\frac{\overline{D}}{\overline{D}t}(V_{\beta k}) \\ &= \rho P_{\alpha\beta} + D^{\nu}_{\alpha\beta} + D^{t}_{\alpha\beta} + D^{p}_{\alpha\beta} + \rho\Phi_{\alpha\beta} - \rho\epsilon_{\alpha\beta},\end{aligned}$$

where $\underline{\underline{V}}$ stands for an eigen-basis of $\underline{\underline{R}}$, $\frac{\overline{D}}{\overline{D}t}(V_{\alpha i})V_{ki}R_{k\beta} + R_{\alpha i}V_{ik}\frac{\overline{D}}{\overline{D}t}(V_{\beta k})$ accounts for total variation of principal direction of $\underline{\underline{R}}$ with respect to time. Einstein conventions holds for repeated Latin indices only. Speziale et al. (1994) stated that for any symmetric real tensor $\underline{\underline{T}}$, the total derivative in its own eigen-basis writes:

$$\left(\frac{\overline{D}}{\overline{D}t}\underline{\underline{T}}\right)_{\alpha\beta} = \frac{\overline{D}}{\overline{D}t}\left(T_{\alpha\beta}\right) + e_{\alpha\gamma\delta}\Omega_{\gamma}T_{\delta\beta} + e_{\beta\gamma\delta}\Omega_{\gamma}T_{\delta\alpha}, \tag{A.7}$$

with $e_{\alpha\beta\gamma}$ the permutation index and $\underline{\Omega}$ the angular velocity at which eigen-vector are rotating. Since tensor $\underline{\underline{R}}$ is symmetric and real valued, the case $\alpha = \beta$ needs to be considered only. Contributions from the rotating frame vanish.

*Non-realizability of the LRR-IP model.* Examples of non realizable flows is presented in a NASA report provided by Shih and Shabbir (1994) for the IP Naot et al. (1970) and LRR-IP Launder et al. (1975) models. An incompressible flow and homogeneous turbulence are considered. Hence, the LRR-IP model writes as:

$$\frac{\overline{D}}{\overline{D}t}(R_{\alpha\alpha}) = (1 - C_2)\,P_{\alpha\alpha} - C_1\frac{\epsilon}{k}\left(R_{\alpha\alpha} - \frac{2}{3}k\right) + C_2\frac{2}{3}P - \frac{2}{3}\epsilon. \tag{A.8}$$

Now departing from realizable initial and boundary conditions, let us consider the case where $R_{\alpha\alpha} \to 0$ (flow converges toward two-dimensional turbulent state). Since $R_{\alpha k} = 0$ for $k \neq \alpha$ and $P_{\alpha\alpha} = -2\rho R_{\alpha k}\dfrac{\partial u_k}{x_\alpha} \underset{R_{\alpha\alpha}\to 0}{\to} 0$ equation (A.8) writes in the limit as:

$$\frac{\overline{D}}{\overline{D}t}(R_{\alpha\alpha}) = (C_1 - 1)\,\frac{2}{3}\epsilon + C_2\frac{2}{3}P. \tag{A.9}$$

First term on the right-hand-side of equation (A.9) is always positive whatever the flow conditions. However second term may become negative as underlined in Shih and Shabbir (1994). Necessary condition for LRR-IP model to be realizable is

to satisfy weak form of realizability (A.1). It leads to:

$$P^\star = \frac{P}{\epsilon} \geq \frac{1 - C_1}{C_2} = -\frac{4}{3}. \tag{A.10}$$

Under most of the flow conditions, this criteria is verified. However under specific conditions, such as shear stress flows, model may become non-realizable as shown by Shih and Shabbir (1994).

## Appendix B. Analytical solutions of the algebraic models

For the sake of completeness and to facilitate the verification procedure, we re-derive algebraic solutions for homogeneous and statistically steady turbulent shear flows, mainly following Pope (2000).

### *Appendix B.1. General formulation*

Algebraic models in turbulence modelling rely on the weak-equilibrium hypothesis, which states that for homogeneous and steady turbulence, convection and diffusion terms of turbulent structures are at equilibrium. When it comes to steady and homogeneous shear flows, weak-equilibrium hypothesis holds exactly. In a DRSM context, Pope (1975) stated that weak-equilibrium hypothesis corresponds to:

$$\frac{\overline{D}}{\overline{D}t}\underline{b} - \underline{\underline{D}}(\underline{b}) = \underline{0} \Rightarrow k\left(\frac{\overline{D}}{\overline{D}t}\underline{\underline{R}} - \underline{\underline{D}}(\underline{\underline{R}})\right) = \left(\frac{\overline{D}k}{\overline{D}t} - D(k)\right)\underline{\underline{R}}, \tag{B.1}$$

with $\underline{b} = \frac{1}{2k}\underline{\underline{R}} - \frac{1}{3}\underline{1}$ the non-dimensional anisotropy tensor and $\underline{\underline{D}} = \underline{\underline{D}}_t(\underline{b}) + \underline{\underline{D}}_\nu(\underline{b}) + \underline{\underline{D}}_p(\underline{b})$ accounting for the sum of the model's diffusion terms. This is equivalent to: For a general DRSM with general form (3), this relation yields:

$$k\left(\underline{\underline{P}} + \underline{\underline{\Phi}} + \underline{\underline{G}} - \underline{\underline{\varepsilon}}\right) = \underline{\underline{R}}\left(P + G - 2\varepsilon\right), \tag{B.2}$$

since $\mathrm{tr}(\underline{\underline{\Phi}}) = 0$ for both exact and modelled terms. For incompressible flows and in the absence of gravity forces: $\beta = 0$ and $\underline{\underline{G}} = \underline{\underline{0}}$. Equation (B.2) reduces to:

$$k\left(\underline{\underline{P}} + \underline{\underline{\Phi}} - \underline{\underline{\varepsilon}}\right) = \underline{\underline{R}}\left(P - \varepsilon\right). \tag{B.3}$$

Terms arising in equation (B.3) are functions only of the turbulent anisotropy tensor, rate of strain tensor and curl tensor. Which yields with LRR-IP model for

the velocity-pressure correlations term:

$$\underline{\underline{\Phi}} = -2C_1\varepsilon\underline{\underline{b}} - C_2\underline{\underline{P}} + \frac{C_2}{3}\mathrm{tr}\underline{\underline{P}}\,\underline{\underline{1}},\ \ \underline{\underline{P}} = -2k\left(\underline{\underline{b}}\cdot\underline{\underline{S}} + \underline{\underline{S}}\cdot\underline{\underline{b}} + \underline{\underline{\Omega}}\cdot\underline{\underline{b}} - \underline{\underline{b}}\cdot\underline{\underline{\Omega}} + \frac{2}{3}\underline{\underline{S}}\right),\ \ \underline{\underline{\varepsilon}} = \frac{2}{3}\varepsilon\underline{\underline{1}}$$

The following equation for $\underline{\underline{b}}$ is obtained:

$$\left(C_1 - 1 + P^\star\right)\underline{\underline{b}} = -\left(1 - C_2\right)\left(\underline{\underline{b}}\,\underline{\underline{S}}^\star + \underline{\underline{S}}^\star\underline{\underline{b}} - \underline{\underline{b}}\cdot\underline{\underline{\Omega}}^\star + \underline{\underline{\Omega}}^\star\cdot\underline{\underline{b}} - \frac{2}{3}Tr\left(\underline{\underline{b}}\cdot\underline{\underline{S}}^\star\right)\underline{\underline{1}} + \frac{2}{3}\underline{\underline{S}}^\star\right), \tag{B.4}$$

with: $C_1 = 1.8$, $C_2 = 0.6$, $P^\star = \frac{\mathrm{tr}(\underline{\underline{P}})}{2\varepsilon} = -2\mathrm{tr}\left(\underline{\underline{b}}\cdot\underline{\underline{S}}^\star\right)$, $\underline{\underline{S}}^\star = \tau\underline{\underline{S}}$ and $\underline{\underline{\Omega}}^\star = \tau\underline{\underline{\Omega}}$. One notices that non-dimensional number $P^\star$ and characteristic time-scale $\tau = \frac{k}{\varepsilon}$ are steady and obtained analytically.

*Appendix B.2. Algebraic model for homogeneous and steady shear flows*

Under shear flow conditions, a homogeneous one-component velocity gradient is imposed and an algebraic analytical solution is obtained for the anisotropy tensor as shown in Pope (1975). Stationary velocity gradient $\underline{\underline{\nabla u}} = Se_x \otimes e_z$ is considered. In addition, turbulence is assumed to be homogeneous, so that the gradients of the turbulent quantities such as $\underline{\underline{R}}$, k and $\varepsilon$ are null. Hence, convection and diffusion terms are equal to zero and the following set of algebraic equations for $k$ and $\varepsilon$ is derived:

$$\frac{\partial\left(\rho k\right)}{\partial t} = \rho\left(P - \varepsilon\right), \qquad \frac{\partial\left(\rho\varepsilon\right)}{\partial t} = \frac{\rho}{\tau}\left(C_{\varepsilon,1}P - C_{\varepsilon,2}\varepsilon\right). \tag{B.5}$$

By considering equation (B.4), $\underline{\underline{b}}$ depends only on $\underline{\underline{S}}$ and $\underline{\underline{\Omega}}$, $\underline{\underline{b}} = \underline{\underline{b}}(\underline{\underline{S}}, \underline{\underline{\Omega}})$. Hence, general formulation of the anisotropy tensor is:

$$\underline{\underline{b}} = \sum_i \sum_{\alpha_i} \sum_j \sum_{\beta_j} G^{\alpha_1,\alpha_2,\ldots,\alpha_i}_{\beta_1,\beta_2,\ldots,\beta_j}\,\underline{\underline{S}}^{\alpha_1}\cdot\underline{\underline{\Omega}}^{\beta_1}\ldots\underline{\underline{S}}^{\alpha_i}\cdot\underline{\underline{\Omega}}^{\beta_j} \tag{B.6}$$

with $G^{\alpha_1,\alpha_2,\ldots,\alpha_i}_{\beta_1,\beta_2,\ldots,\beta_j}$ function of the invariants $\mathrm{tr}\left(\underline{\underline{S}}^{\alpha_1}\cdot\underline{\underline{\Omega}}^{\beta_1}\ldots\underline{\underline{S}}^{\alpha_i}\cdot\underline{\underline{\Omega}}^{\beta_j}\right)$. Using Caylay-Hamilton theorem, Pope (1975) stated that for two-dimensional flows $\underline{\underline{b}}$ is a function only of three independent tensor invariants:

$$\underline{\underline{T}}^1 = \left(\frac{1}{3}\underline{\underline{I}}_3 - \frac{1}{2}\underline{\underline{I}}_2\right), \qquad \underline{\underline{T}}^2 = \underline{\underline{S}}, \qquad \underline{\underline{T}}^3 = \underline{\underline{S}}\cdot\underline{\underline{\Omega}} - \underline{\underline{\Omega}}\cdot\underline{\underline{S}},$$

and two independent scalar invariants: $\mathrm{tr}(\underline{\underline{S}}\cdot\underline{\underline{S}})$ and $\mathrm{tr}(\underline{\underline{\Omega}}\cdot\underline{\underline{\Omega}})$. $\underline{\underline{I}}_3$ and $\underline{\underline{I}}_2$ stands for the identity tensor in dimensions three and two prolongated with zeros, respectively.

Solution is searched in the basis made of tensors ($\underline{\underline{T}}^1$, $\underline{\underline{T}}^2$, $\underline{\underline{T}}^3$). It has the general form:

$$\underline{\underline{b}} = \alpha\underline{\underline{T}}^1 + \beta\underline{\underline{T}}^2 + \gamma\underline{\underline{T}}^3. \tag{B.7}$$

Making use of equation (B.7), analytical solution for the LRR-IP writes:

$$\underline{\underline{b}} = \begin{pmatrix} \frac{\frac{4}{9}(1-C_2)^2 S^{\star 2}}{(C_1-1+P^\star)^2+(1-C_2)^2\frac{2}{3}S^{\star 2}} & 0 & \frac{-\frac{1}{3}(1-C_2)(C_1-1+P^\star)S^\star}{(C_1-1+P^\star)^2+(1-C_2)^2\frac{2}{3}S^{\star 2}} \\ 0 & \frac{-\frac{2}{9}(1-C_2)^2 S^{\star 2}}{(C_1-1+P^\star)^2+(1-C_2)^2\frac{2}{3}S^{\star 2}} & 0 \\ \frac{-\frac{1}{3}(1-C_2)(C_1-1+P^\star)S^\star}{(C_1-1+P^\star)^2+(1-C_2)^2\frac{2}{3}S^{\star 2}} & 0 & \frac{-\frac{2}{9}(1-C_2)^2 S^{\star 2}}{(C_1-1+P^\star)^2+(1-C_2)^2\frac{2}{3}S^{\star 2}} \end{pmatrix}. \tag{B.8}$$

The analytical solution depends on the production to dissipation ratio $P^\star$ and integral time-scale $\tau$ which are fully determined under weak-equilibrium hypothesis. Algebraic models implicitly suppose stationarity of the turbulent structures. Hence, the time derivatives of the characteristic turbulent quantities vanish under weak-equilibrium hypothesis. Considering $\tau$, the integral turbulent time-scale:

$$\frac{\partial \tau}{\partial t} = \frac{1}{\varepsilon}\frac{\partial k}{\partial t} - \frac{k}{\varepsilon^2}\frac{\partial \varepsilon}{\partial t} = 0. \tag{B.9}$$

Using equations (B.5) and (B.9) the steady $P^\star$ obtained from weak-equilibrium is:

$$P^\star = \frac{C_{\varepsilon 2} - 1}{C_{\varepsilon 1} - 1}. \tag{B.10}$$

Now, let us derive $\tau$ at equilibrium. From the definition of $P^\star$:

$$P^\star = -2\mathrm{tr}\left(\underline{\underline{b}} \cdot \underline{\underline{S}}^\star\right) = -4\tau b_{xz} S_{xz}. \tag{B.11}$$

Replacing $b_{xz}$ by the steady solution (B.8) and making use of positivity of both $\tau$ and $P^\star$:

$$\tau = \frac{\sqrt{3}}{2\sqrt{2}}\sqrt{\frac{P^\star\left(C_1 - 1 + P^\star\right)^2}{\left(C_1 - 1 + P^\star C_2\right)(1-C_2)S_{xz}^2}}. \tag{B.12}$$

Turbulent time-scale is a function only of the DRSM constants (see Table 2) and the shear stress magnitude.

One can notice that solution (B.8) gives a Reynolds stress SPD for any conditions.